



Published in final edited form as:

Cell Rep. 2021 May 25; 35(8): 109184. doi:10.1016/j.celrep.2021.109184.

The autophagy protein Becn1 improves insulin sensitivity by promoting adiponectin secretion via exocyst binding

Kenta Kuramoto¹, Yoon-Jin Kim¹, Jung Hwa Hong¹, Congcong He^{1,2,*}

¹Department of Cell and Developmental Biology, Feinberg School of Medicine, Northwestern University, Chicago, IL 60611, USA

²Lead contact

SUMMARY

Autophagy dysregulation is implicated in metabolic diseases, including type 2 diabetes. However, the mechanism by which the autophagy machinery regulates metabolism is largely unknown. Autophagy is generally considered a degradation process via lysosomes. Here, we unveil a metabolically important non-cell-autonomous, non-degradative mechanism regulated by the essential autophagy protein Becn1 in adipose tissue. Upon high-fat diet challenge, autophagy-hyperactive Becn1^{F121A} mice show systemically improved insulin sensitivity and enhanced activation of AMP-activated protein kinase (AMPK), a central regulator of energy homeostasis, via a non-cell-autonomous mechanism mediated by adiponectin, an adipose-derived metabolic hormone. Adipose-specific Becn1^{F121A} expression is sufficient to activate AMPK in non-adipose tissues and improve systemic insulin sensitivity by increasing adiponectin secretion. Further, Becn1 enhances adiponectin secretion by interacting with components of the exocyst complex via the coiled-coil domain. Together, our study demonstrates that Becn1 improves insulin sensitivity by facilitating adiponectin secretion through binding the exocyst in adipose tissue.

In brief

Kuramoto et al. demonstrate a non-degradative and non-cell-autonomous mechanism by which the autophagy protein Becn1 regulates systemic energy metabolism. Becn1 interacts with exocyst proteins in white adipose tissue to facilitate adiponectin secretion, resulting in systemic insulin sensitization via the adiponectin receptor-AMPK signaling pathway in non-adipose tissues.

Graphical Abstract

This is an open access article under the CC BY-NC-ND license (<http://creativecommons.org/licenses/by-nc-nd/4.0/>).

*Correspondence: congcong.he@northwestern.edu.

AUTHOR CONTRIBUTIONS

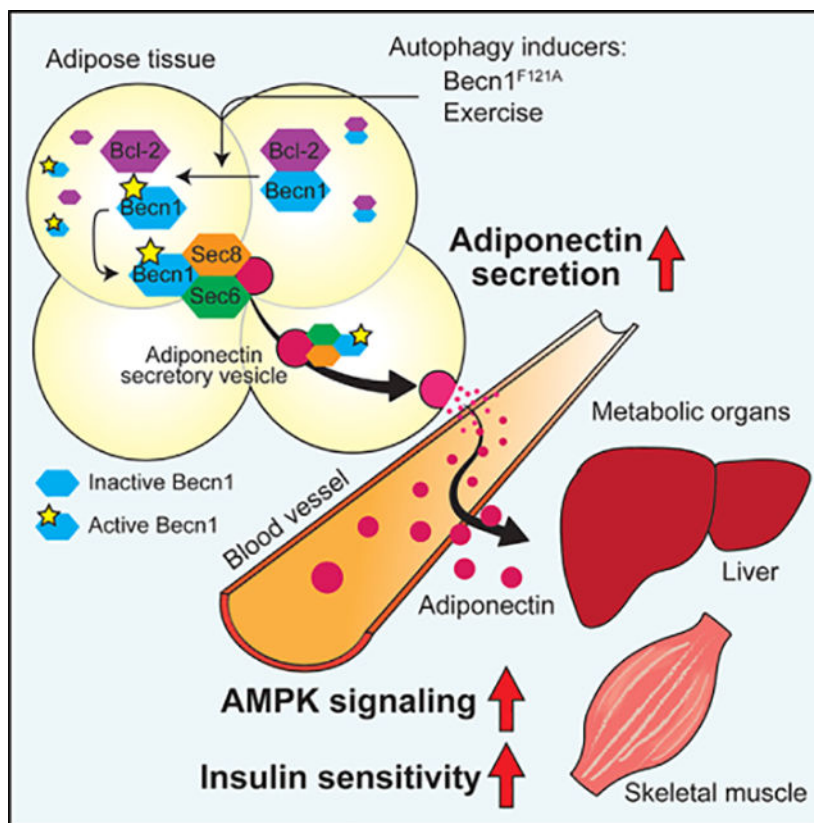
K.K. and C.H. conceived the project and designed the experiments. K.K., Y.-J.K., and J.H.H. performed the experiments. K.K. and C.H. analyzed the data. K.K. and C.H. wrote the manuscript.

DECLARATION OF INTERESTS

The authors declare no competing interests.

SUPPLEMENTAL INFORMATION

Supplemental information can be found online at <https://doi.org/10.1016/j.celrep.2021.109184>.



INTRODUCTION

Autophagy is a key lysosomal degradation pathway induced by stress, such as fasting and exercise, which breaks down damaged or unnecessary structures by fusion of autophagosome vesicles with lysosomes (Kaur and Debnath, 2015; Rocchi and He, 2017b). Deletion of autophagy genes in mice, either globally or specifically in metabolic tissues, including pancreatic β cells and liver, has been linked with metabolic dysfunctions, such as hyperglycemia and insulin resistance, the hallmarks of type 2 diabetes (T2D) (Ebato et al., 2008; He et al., 2013; Jung et al., 2008; Rocchi and He, 2015; Yang et al., 2010). In contrast, recent data indicate that both physiological and genetic activation of autophagy increases insulin sensitivity (He et al., 2012; Yamamoto et al., 2018). However, the mechanism by which the autophagy machinery regulates insulin sensitivity and T2D pathogenesis remains obscure. Autophagy is generally considered a destruction and degradation process. Although emerging evidence suggests that autophagy may have an unconventional secretory function in immunity and inflammation (Bel et al., 2017; Zhang et al., 2015), whether autophagy-related proteins play non-degradative roles in the regulation of metabolism, as well as the underlying mechanisms, is unknown.

Besides serving as lipid storages, adipose tissue is an important endocrine organ that regulates energy metabolism in various metabolic tissues via secreting adipokines (adipose-derived hormones), including adiponectin. Adiponectin regulates a spectrum of metabolic parameters in the muscle, liver, and vascular system, including maintaining insulin

sensitivity, promoting free fatty acid oxidation, reducing hepatic glucose and triglyceride (TG) production, and inhibiting vascular inflammation (Kadowaki et al., 2006; Ouchi et al., 2011; Stern et al., 2016; Yamauchi et al., 2001). The expression and plasma concentration of adiponectin positively correlates with insulin sensitivity and is reduced in obesity and T2D in both animal models and humans (Arita et al., 1999; Hotta et al., 2001; Li et al., 2009). Low blood adiponectin caused by SNPs (single-nucleotide polymorphisms) or mutations in the *Adiponectin* gene in humans, also known as hypoadiponectinemia, has been associated with insulin resistance and T2D (Hara et al., 2002; Kondo et al., 2002; Menzaghi et al., 2002; Stumvoll et al., 2002). Adiponectin knockout (KO) mice phenocopy the human phenotypes and develop insulin resistance (Kubota et al., 2002; Nawrocki et al., 2006), demonstrating the key role of adiponectin in the prevention of T2D. Thus, understanding factors that regulate the endocrine pathway of adiponectin secretion in adipose tissue will help elucidate the pathogenesis of insulin resistance and metabolic disorders. However, despite the importance of adiponectin in metabolic homeostasis, the molecular mechanism of adiponectin secretion from adipose tissue is unclear. Although extracellular signals, such as insulin, adrenergic stimuli, and fibroblast growth factor 21 (FGF21) (Blümer et al., 2008; Cong et al., 2007; Geng et al., 2019; Hajri et al., 2011; Holland et al., 2013; Komai et al., 2016; Lim et al., 2015; Lin et al., 2013), have been reported to increase adiponectin release in adipocytes via corresponding receptors, the intracellular mechanism that controls the secretion of adiponectin after it is folded and packaged in the endoplasmic reticulum (ER) is poorly defined.

Becn1/Becn1 is an essential autophagy protein that binds the class III Vps34 phosphatidylinositol 3-kinase (PtdIns3K) complex and regulates its stability and kinase activity during autophagy initiation (He and Levine, 2010). Becn1 is reported to be required for exercise-induced activation of AMPK (AMP-activated protein kinase), a central positive regulator of insulin sensitivity and glucose uptake, in muscle via binding with the Toll-like receptor 9 (TLR9) (He et al., 2012; Liu et al., 2020). We recently established a Becn1 mutant mouse model of hyperactive autophagy, Becn1^{F121A} knockin (KI) mice, to study the role and mechanism of autophagy in metabolic regulation (Rocchi et al., 2017; Yamamoto et al., 2018). The Becn1^{F121A} point mutant cannot be bound and inhibited by the anti-apoptotic and anti-autophagy protein Bcl-2 and leads to high autophagy. Becn1^{F121A}-mediated genetic upregulation of autophagy improves systemic insulin sensitivity, but the mechanism by which autophagy regulates insulin sensitivity is unclear.

In this study, we found that Becn1 regulates metabolism through a previously uncharacterized non-degradative, non-cell-autonomous mechanism by regulating adiponectin secretion from adipocytes. The autophagy-hyperactive Becn1^{F121A} mutation mimics the effect of exercise on AMPK activation and leads to systemic AMPK activation at resting conditions. This effect is exerted by a non-cell-autonomous mechanism mediated by autophagy-induced circulating adiponectin from adipocytes, because adipose tissue-specific expression of Becn1^{F121A} is sufficient to increase liver and muscle AMPK activation, circulating adiponectin levels, and systemic insulin sensitivity, which is abolished by reduced adiponectin expression. Mechanistically, we discovered that an interaction between Becn1 and the exocyst components in adipocytes is required for Becn1^{F121A}-induced secretion of adiponectin. Altogether, we establish a model of Becn1-facilitated adiponectin

secretion in adipose tissue: when the essential autophagy protein Becn1 is released from the inhibitory binding of Bcl-2, it promotes adiponectin secretion via binding to the exocyst complex in adipose tissue, which elevates circulating adiponectin, activates AMPK in target metabolic tissues, and increases insulin sensitivity systemically (Figure 7G).

RESULTS

Autophagy-hyperactive *Becn1*^{F121A} mice show systemic AMPK activation in metabolic tissues caused by circulator factors

To study how autophagy regulates metabolism, we previously generated an autophagy-hyperactive KI mouse model carrying a single amino acid substitution (F121A) in the *Becn1* protein (*Becn1*^{F121A}), which disrupts inhibitory binding between *Becn1* and Bcl-2 and leads to constitutive activation of autophagy (Rocchi et al., 2017). We found that in response to 8- or 12-week high-fat diet (HFD) feeding, while *Becn1*^{F121A} mice showed comparable body weight to wild-type (WT) mice, they are less glucose tolerant yet more insulin sensitive than WT mice (Yamamoto et al., 2018) (Figure S1A). Our previous findings suggest that after HFD challenge, the *Becn1*^{F121A} mice showed excessive autophagic degradation of insulin granule vesicles (vesicophagy) in β cells, leading to impaired insulin secretion and glucose intolerance. However, it does not explain why *Becn1*^{F121A} mice are paradoxically more insulin sensitive. To solve this puzzle, we analyzed various metabolic pathways in their metabolic tissues and found that compared with WT mice, metabolic tissues (liver and skeletal muscle) of *Becn1*^{F121A} mice showed enhanced phosphorylation/activation of AMPK, which plays a central beneficial role in energy homeostasis and insulin sensitization (Garcia and Shaw, 2017), after feeding of either regular diet (RD) (Figure 1A) or HFD (Figure 1B). Further, in support of AMPK activation, *Becn1*^{F121A} mouse tissues showed a spectrum of changes downstream of AMPK, including increased phosphorylation of Raptor (Regulatory-associated protein of mTOR [mechanistic target of rapamycin]), decreased phosphorylation of p70S6K and IRS-1 (Insulin receptor substrate 1), and stabilization of IRS-1 (Figure 1B). AMPK phosphorylates Raptor at S792, which leads to inhibition of mTOR and its substrate p70S6K (Gwinn et al., 2008). The latter can phosphorylate IRS-1 at several serine residues, including S302 and S632/635 (Haruta et al., 2000; Ozes et al., 2001; Ueno et al., 2005; Werner et al., 2004), which promotes IRS-1 degradation via proteasomes (Pederson et al., 2001; Sun et al., 1999; Takano et al., 2001). Because IRS-1 is a key docking protein downstream of the activated insulin receptor (IR) and insulin-like growth factor-1 receptor (IGF-1R) to form scaffolding complexes and initiate insulin signaling cascades, stabilization of IRS-1 by AMPK activation in part enhances insulin sensitivity. Thus, more Raptor S792 phosphorylation, less p70S6K T389 phosphorylation, less IRS1 S302 and S632/635 phosphorylation, and higher levels of IRS-1 in the metabolic tissues of *Becn1*^{F121A} mice suggest an activated AMPK signaling pathway in these mice (Figure 1B).

Notably, WT *Becn1* is reported to be required for exercise-induced activation of AMPK in muscle via binding with TLR9 (He et al., 2012; Liu et al., 2020). Thus, the hyperactive *Becn1*^{F121A} mutation mimics the effect of exercise on AMPK activation at resting conditions. Intriguingly, this effect is not due to differences in the level of TLR9 (Figure S1B) and is not limited to muscle (Figures 1A and 1B). To reveal the mechanism underlying

AMPK hyperactivation in *Becn1*^{F121A} mice, we asked whether AMPK activation is caused by a cell-autonomous or non-cell-autonomous mechanism. We added 10% serum collected from either WT or *Becn1*^{F121A} mice to the medium of WT cells of metabolic tissue origins. We found that when added to cell culture media, serum from *Becn1*^{F121A} mice also leads to enhanced AMPK activation in various cell lines (including NIH 3T3 fibroblasts, HepG2 and Huh7 hepatocytes, C2C12 myotubes, and 3T3-L1 preadipocyte-differentiated adipocytes), compared with serum from WT mice or the PBS control (Figures 1C and S1C). In contrast, primary cells isolated from WT and *Becn1*^{F121A} mice, including primary MEFs (mouse embryonic fibroblasts) and primary hepatocytes, did not show differences in AMPK activation in the absence or presence of the AMPK activator AICAR (Figure S1D). These data suggest that *Becn1*^{F121A}-induced AMPK-activating, as well as insulin-sensitizing, effects are likely mediated by a non-cell-autonomous mechanism through circulating factors.

***Becn1*^{F121A} mice have increased circulating levels of adiponectin**

To identify the *Becn1*-controlled circulating factor that has an AMPK-activating and potentially insulin-sensitizing effect, we did a Luminex array (Millipore) on metabolic hormones in the serum of WT and *Becn1*^{F121A} mice (Figure S2A, showing partial data). We detected a higher circulating level of adiponectin, but not other metabolic hormones tested, in *Becn1*^{F121A} mice than in WT littermates in response to either RD or HFD feeding (Figure 2A). We confirmed that *Becn1*^{F121A} mice have elevated circulating adiponectin by western blot (WB) analysis (Figure 2B), despite comparable body weight, white adipose tissue (WAT) mass (Figure S2B), intra-tissue adiponectin levels (Figure S2C), and circulating levels of the adiponectin secretagogue FGF21 (Figure S2D) with those of WT mice. In addition, we found that *Becn1* heterozygous KO mice have reduced serum adiponectin compared with WT littermates (Figure 2C), further supporting the role of *Becn1* in the regulation of circulating adiponectin levels.

Adiponectin exists in the circulation as different multimer complexes, categorized as high-molecular-weight (HMW) multimers, medium-molecular-weight (MMW) hexamers, and low-molecular-weight (LMW) trimers, with the HMW adiponectin being the most biologically active form (Basu et al., 2007; Lara-Castro et al., 2006; Murdolo et al., 2009; Pajvani et al., 2004). We found that the HMW and MMW forms of adiponectin show a significant increase in the serum of *Becn1*^{F121A} mice, using ELISA (Figure 2A) and an antibody that detects the total and HMW adiponectin (Figure 2D) or another antibody that detects the MMW, but not the HMW, form of adiponectin (Figure S2E). Further, we found that increased adiponectin secretion from *Becn1*^{F121A} adipocytes is cell autonomous, because there is more adiponectin secreted into the medium from *in vitro*-cultured primary adipocytes isolated from *Becn1*^{F121A} mice (Figure 2E) or from *Becn1*^{F121A}-expressing 3T3-L1-differentiated adipocytes (Figure S2F). Together, these data suggest that *Becn1*^{F121A} induces adiponectin secretion, mediated by a cell-autonomous mechanism.

***Becn1*^{F121A}-induced adiponectin signaling is essential for non-cell-autonomous AMPK activation**

Adiponectin activates several intracellular targets, including AMPK signaling, via binding and signaling through the membrane receptors adiponectin receptor 1 (AdipoR1) and

AdipoR2 in metabolic tissues, such as liver and muscle (Wu et al., 2003; Yamauchi et al., 2002; Yoon et al., 2006). To determine whether AMPK activation in *Becn1*^{F121A} mice is dependent on increased secretion of adiponectin, we asked whether depleting adiponectin receptors in non-adipose cells abolishes AMPK activation induced by *Becn1*^{F121A} mouse serum. We found that compared with WT mouse serum, serum from *Becn1*^{F121A} mice led to higher AMPK activation in WT C2C12 myotubes but failed to do so in C2C12 myotubes deleted for the adiponectin receptor AdipoR1 (the major adiponectin receptor expressed in myotubes) by short hairpin RNAs (shRNAs) (Figure 3A). Similarly, we also found that the adiponectin receptors are required for *Becn1*^{F121A} mouse serum-induced AMPK activation in NIH 3T3 fibroblasts (primarily expressing AdipoR1) (Figure 3B) and 3T3L1-differentiated adipocytes (expressing both AdipoR1 and AdipoR2) (Figure S3). These data suggest that adiponectin signaling is required for AMPK activation in target metabolic cells induced by *Becn1*^{F121A} mouse serum.

The exocyst components Sec5, Sec6, and Sec8 are binding partners of Becn1 and preferentially interact with the hyperactive Becn1^{F121A} mutant compared with WT Becn1

We next aimed to understand how the autophagy machinery cell autonomously regulates adiponectin secretion in adipocytes. Indeed, we found that the WAT of the *Becn1*^{F121A} mice shows disrupted Becn1-Bcl-2 interaction, assayed by co-immunoprecipitation (coIP) (Figure 4A), as well as increased autophagy activity, evidenced by elevated LC3-II and p62 flux using a lysosomal inhibitor chloroquine (Figure S4A). Nonetheless, we did not detect elevated or accelerated adipogenesis in the WAT of *Becn1*^{F121A} mice (Figure 4B), in primary adipocytes from *Becn1*^{F121A} mice (Figure S4B), or in *Becn1*^{F121A}-expressing 3T3-L1-differentiated adipocytes (Figures 4C and S4C), by analyzing the expression of a variety of adipogenesis markers. The data suggest that upregulating autophagy by *Becn1*^{F121A} does not affect adipose development and differentiation. We then suspected that autophagosomes may directly sequester adiponectin and promote its secretion, because we previously found that under certain conditions hormones can become an autophagy cargo (Kuramoto and He, 2018; Yamamoto et al., 2018). However, our imaging and biochemical data ruled out this possibility as well. We did not observe significant colocalization between adiponectin and the autophagosome marker LC3 in primary adipocytes of either WT GFP-LC3 or *Becn1*^{F121A} GFP-LC3 reporter mice by confocal microscopy (Figure S4D). Moreover, using a biochemical method we developed to immunoprecipitate intact autophagosomes from cells and tissues (Yamamoto et al., 2018), we did not detect adiponectin inside autophagosomes purified from 3T3-L1-differentiated adipocytes (Figure S4E). Thus, these data suggest that adiponectin elevation in *Becn1*^{F121A} KI mice is not due to altered adipogenesis or enhanced sequestration and secretion of adiponectin directly by autophagosome vesicles.

Nonetheless, we detected colocalization between adiponectin and Becn1 in primary adipocytes and a higher level of colocalization of adiponectin with *Becn1*^{F121A} than with WT Becn1 (Figure 5A), supporting that Becn1 may play a direct role in regulating adiponectin secretion. To investigate the potential mechanism of Becn1-regulated adiponectin release, we generated a HEK293 cell line stably expressing a tetracycline-inducible cleavable zz tag-Becn1-3XFlag fusion protein (Sun et al., 2008). Using this cell line, we pulled down several subunits of the exocyst as Becn1 binding partners, including

Sec5/Exoc2, Sec6/Exoc3, and Sec8/Exoc4 (Figure S5A). In the meantime, when we interrogated published databases and reports of the Becn1 interactome, we found that another exocyst component Exo84/Exoc8 has been reported as a Becn1-binding protein (Bodemann et al., 2011). The exocyst is a multiprotein complex involved in plasma-membrane docking of secretory vesicles, containing eight components: Sec3/Exoc1, Sec5/Exoc2, Sec6/Exoc3, Sec8/Exoc4, Sec10/Exoc5, Sec15/Exoc6, Exo70/Exoc7, and Exo84/Exoc8 (Heider and Munson, 2012; Wu and Guo, 2015). By coIP, we confirmed the interaction of the key exocyst component Sec6 with both WT Becn1 and Becn1^{F121A} in HEK293 cells (Figure 5B) and found that the hyperactive mutant form, Becn1^{F121A}, shows a higher affinity with Sec6 than WT Becn1 in HEK293 cells stably expressing WT Becn1 or Becn1^{F121A} (Figures 5B and 5C), in primary adipocytes isolated from WT or Becn1^{F121A} mice (Figure 5D), and in 3T3-L1-differentiated adipocytes (Figure S5B). Different from the previous report (Bodemann et al., 2011), we were not able to detect an interaction between Becn1 and the exocyst components Exo84 or Exo70 in HEK293 cells (Figure 5B), but we found that in the presence of Becn1^{F121A}, there is a stronger binding between Sec6 and several other exocyst components, such as Sec5 and Sec8 (Figure 5C). Further, in addition to Sec6, the exocyst components Sec5 and Sec8, as well as PtdIns3K complex subunits ATG14, VPS34, and UVRAG, also show stronger binding with Becn1^{F121A} than with WT Becn1 analyzed by coIP in primary adipocytes (Figure 5D). Together, these data suggest that Becn1 binds the exocyst complex and facilitates exocyst assembly, and the exocyst machinery preferentially interacts with the hyperactive Becn1^{F121A} mutant compared with WT Becn1.

The Becn1-exocyst interaction is essential for promoting adiponectin secretion

To further determine whether the Becn1-Sec6 interaction is important for adiponectin secretion, we aimed to generate a loss-of-Sec6 interaction mutant of Becn1. Becn1 contains three major domains: the BH3 (Bcl-2 homology 3) domain that binds Bcl-2, the coiled-coil domain (CCD), and the evolutionally conserved domain (ECD) (He and Levine, 2010; Levine et al., 2015). We generated deletion mutants of Becn1^{F121A} lacking the N-terminal intrinsically disordered region, the BH3 domain, the CCD, the ECD, or the C-terminal regions, respectively (Figure 5E). We found that the Becn1 CCD mutant (lacking the CCD) disrupts the Becn1-Sec6 binding by coIP (Figure 5E), suggesting that the CCD of Becn1 is important for exocyst binding. We subsequently stably expressed full-length Becn1^{F121A} and the loss-of-Sec6 interaction Becn1^{F121A} CCD mutant in WT 3T3-L1 preadipocytes, induced adipocyte differentiation of the 3T3-L1 cells, and analyzed adiponectin levels in the conditioned medium. We found that Becn1^{F121A} CCD abolishes the increase in the medium adiponectin level induced by Becn1^{F121A} and by WB (Figure 5F) and ELISA (Figure 5G) analyses, suggesting that disrupting Becn1-Sec6 binding interferes with Becn1-regulated adiponectin secretion in adipocytes. Thus, we conclude that Becn1 regulates adiponectin secretion by interacting with the exocyst.

We also demonstrated that the exocyst machinery functions in adiponectin release from adipocytes, which has not been characterized before. We found that shRNA knockdown (KD) of Sec6 significantly decreases the adiponectin level in the conditioned medium of 3T3-L1 preadipocyte-differentiated adipocytes (Figure S5C), suggesting that Sec6 is

required for adiponectin secretion in adipocytes. Yet KD of another exocyst component Sec5 does not affect adiponectin secretion (Figure S5D). This is in line with reported phenomena in *Drosophila*, where mutating Sec5 does not impair the secretion of neurotransmitters (Murthy et al., 2003). Based on the cryoelectron microscopy (cryo-EM) structure of the exocyst (Mei et al., 2018), we speculate that it is possible that Becn1 and Sec5 may be partially functionally redundant in adiponectin secretion, and binding of Becn1 to Sec6 or the exocyst may compensate for the loss of Sec5 in the secretion. We found that KD of Sec8 reduces adiponectin secretion (Figure S5D); yet, depleting Sec8 also reduces the stability of Sec6, consistent with the structural data suggesting that Sec8 forms a paired subcomplex with Sec6 in the exocyst (Mei et al., 2018). These data demonstrate that Sec6 needs to cooperate with Sec8, but not Sec5, to exert its effects on adiponectin secretion.

We also found that Sec6 is partially required for the secretion of another adipokine leptin (Figure S5C). However, intriguingly, we found that different from adiponectin, expressing Becn1^{F121A} or blocking the Becn1-Sec6 binding does not affect the secretion of leptin from 3T3-L1-differentiated adipocytes (Figure 5G). Our microscopy data suggest that this specificity is potentially caused by subcellular compartmentation and distinct trafficking pathways of different types of secretory vesicles. We found that as previously reported (Xie et al., 2008), although adiponectin-containing vesicles are enriched in the internal subcellular pool (center), leptin vesicles mostly localize in proximity to the cell surface (periphery) and show limited colocalization with adiponectin (Figure 5H). In addition, compared with adiponectin vesicles, leptin vesicles have reduced colocalization with Becn1, and such colocalization is not increased by hyperactive Becn1^{F121A} (Figure S5E). Thus, it is likely that various types of vesicles are originated from distinct compartments of the Golgi and trafficked to different subcellular locations that are Becn1 positive or negative. We propose that the Becn1-Sec6 complex forms approximate to adiponectin vesicles at the center of the adipocyte to promote their transport toward the plasma membrane.

Adipose tissue-specific expression of Becn1^{F121A} is sufficient to improve systemic insulin sensitivity, glucose tolerance, and insulin signaling in liver and muscle

To further demonstrate that Becn1 in the WAT is key for adiponectin secretion and metabolic improvement, we compared the metabolic phenotypes of mice expressing Becn1^{F121A} specifically in the WAT or globally in the whole body, to determine whether adipose tissue-specific Becn1^{F121A} expression is sufficient to activate AMPK in non-adipose tissues and improve insulin sensitivity systemically. We utilized the FLEX switch system to deliver Becn1^{F121A} to adipose tissue via adeno-associated virus 2/8 (AAV2/8) (Jimenez et al., 2013) that can efficiently target adipose tissues. In the FLEX system, the Becn1^{F121A} reading frame is reversed and flanked by loxP and lox2272 sites (Figure 6A). When AAV2/8-FLEX-Becn1^{F121A} is injected into WT mice (without Cre expression), Becn1^{F121A} is not expressed, while when AAV2/8-FLEX-Becn1^{F121A} is injected into an adipose-specific Adiponectin-Cre (Adipoq-Cre) mouse line (Cre driven by the adiponectin promoter), the Becn1^{F121A} reading frame is flipped following Cre-Lox recombination and expresses specifically in adipose tissues. Using this system, we confirmed the expression specificity of Becn1^{F121A} after AAV delivery in both inguinal WAT (iWAT) and gonadal WAT (gWAT), but not liver, of Adipoq-Cre mice (Figures 6A and S6A).

With RD feeding, we found that Adipoq-Cre mice injected with AAV-FLEX-Becn1^{F121A} (Adipoq-Cre AAV-Becn1^{F121A} mice) have similar body weight (Figure S6B), insulin sensitivity (by insulin tolerance test [ITT]), and glucose tolerance (by glucose tolerance test [GTT]) (Figure S6C) as the control (WT AAV-Becn1^{F121A}) mice. Yet, in response to HFD feeding, although Adipoq-Cre AAV-Becn1^{F121A} mice have comparable body weight (Figure S6B) and WAT mass (Figure S6D) with the control mice, they show significantly improved insulin sensitivity similar to the global Becn1^{F121A} KI mice (Figure 6B), suggesting that adipose-specific expression of Becn1^{F121A} is sufficient to enhance systemic insulin sensitivity. Importantly, different from global expression of Becn1^{F121A}, which improves insulin sensitivity but impairs glucose tolerance as a result of reducing insulin storage and secretion in islets (Figure S1A) (Yamamoto et al., 2018), adipose tissue-specific Becn1^{F121A} expression improves both insulin sensitivity (ITT) and glucose tolerance (GTT) (Figure 6B, compared with Figure S1A), suggesting an anti-diabetic function of Becn1^{F121A} in adipose tissue.

Along this line, we found that after HFD challenge, control mice showed an abnormally high level of insulin in the serum (hyperinsulinemia) under basal conditions (time 0 min), whereas Adipoq-Cre AAV-Becn1^{F121A} mice showed significantly reduced HFD-induced hyperinsulinemia (Figure 6C). Further, different from whole-body Becn1^{F121A} KI (Yamamoto et al., 2018), adipose tissue-specific expression of Becn1^{F121A} does not cause a reduction in the insulinogenic index (a measure of glucose-stimulated insulin secretion) (Figure S6E), further supporting that previously observed Becn1^{F121A}-induced reduction in insulin secretion is due to its role specifically in β cells. In addition, in support of systemic insulin sensitization, we detected higher phosphorylation of Akt at S473, a phosphorylation target downstream of the activated IR, in both liver and muscle of Adipoq-Cre AAV-Becn1^{F121A} mice than in the control mice, after exogenous insulin stimulation after HFD feeding (Figure 6D), suggesting that Becn1^{F121A} in adipose tissue improves insulin signaling in non-adipose tissues. Thus, together, these findings demonstrate that Becn1^{F121A} is metabolically beneficial and improves systemic insulin sensitivity when specifically expressed in the WAT, and highlight that autophagy proteins may play different roles in different metabolic tissues.

Adipose-specific Becn1^{F121A} regulates AMPK activity and lipid metabolism in non-adipose tissues

We further found that similar to the effect of global Becn1^{F121A} expression (Figure 1B), adipose tissue-specific expression of Becn1^{F121A} is sufficient to activate AMPK in the liver (Figure 6E) and muscle (Figure S6F), evidenced by activated AMPK phosphorylation and downstream signaling of AMPK, including increased phosphorylation of Raptor, decreased phosphorylation of p70S6K and IRS-1, and stabilization of IRS-1. Notably, upon IR activation, IRS-1 is phosphorylated at Y612, which is essential for downstream PtdIns3K activation and GLUT4 translocation. We detected a higher cellular level of Y612 phosphorylation in IRS-1 in Adipoq-Cre AAV-Becn1^{F121A} mice than in control mice (Figure S6G), further supporting liver insulin sensitization mediated non-cell autonomously by adipose Becn1^{F121A}.

Further, adiponectin systemically regulates lipid metabolism by activating AMPK and peroxisome proliferator-activated receptor (PPAR) a signaling pathways via AdipoR2 in the liver (Kadowaki et al., 2006; Yamauchi et al., 2002; Yoon et al., 2006). Activated AMPK inhibits SREBP1 and SREBP2 (sterol regulatory element binding proteins), the master transcription factors of fatty acid biosynthesis (Li et al., 2011). Activation of PPAR α induces gene expression involved in fatty acid oxidation (Haemmerle et al., 2011; Rakhshandehroo et al., 2010). Thus, as the outcome of elevated circulating adiponectin, decreased fatty acid biosynthesis and increased fatty acid oxidation together will lead to reduced liver TG levels. Indeed, compared with control mice, we found that Adipoq-Cre AAV-Becn1^{F121A} mice have significantly decreased liver TG contents (Figure 6F) and, as a result, a reduced level of the lipid droplet coating protein PLIN2 (Perilipin-2) in the liver (Figure 6G), because PLIN2 is stable only on lipid droplets, and cytosolic PLIN2 is degraded by the proteasome pathway (Masuda et al., 2006; Xu et al., 2005). Such reduction in TG and PLIN2 is not due to higher lipophagy in the liver of these mice because the Becn1^{F121A} expression is adipose specific. Rather, in line with increased circulating adiponectin, in response to HFD feeding, we detected a significantly reduced level of the SREBP-target key lipogenesis enzyme ACC (acetyl coenzyme A carboxylase) by WB analysis (Figure 6G) and a trend of increased expression of PPAR α -target fatty acid oxidation genes by qPCR (including peroxisomal acyl-coenzyme A oxidase 1 [*Acox1*], carnitine palmitoyltransferase 1A [*Cpt1a*], uncoupling protein 2 [*Ucp2*], and fatty acid binding protein 1 [*Fabp1*]) (Figure S6H) in the liver of Adipoq-Cre AAV-Becn1^{F121A} mice compared with control mice. These data support that adipose Becn1 non-cell-autonomously regulates AMPK and PPAR α signaling pathways and lipid metabolism in the liver. Together, the findings demonstrate that the activity of Becn1 in the WAT plays an important role in the regulation of systemic glucose and lipid metabolism.

Adipose-specific Becn1^{F121A} increases adiponectin secretion and non-cell-autonomously regulates systemic insulin sensitivity via enhancing adiponectin secretion

We further detected a significantly higher level of circulating adiponectin in Adipoq-Cre AAV-Becn1^{F121A} mice than in control mice in response to HFD treatment, measured by WB analysis (Figure 7A) and ELISA (Figure 7B). The circulating adiponectin level is also increased in adipose-specific Becn1^{F121A} mice fed with RD (Figure S7A), which is similar to global Becn1^{F121A} mice (Figure 2A). Consistent with cell culture studies (Figure 5G), we found that except adiponectin, circulating levels of two other adipokines, leptin and resistin, are comparable in control and adipose-specific Becn1^{F121A} mice after HFD treatment (Figure 7B), further supporting a level of specificity of Becn1 in the regulation of adipokine secretion. These data suggest that adipose tissue-specific Becn1^{F121A} expression is sufficient to increase adiponectin secretion, in support of the cell-autonomous effect of Becn1^{F121A} on adiponectin secretion in primary adipocytes (Figure 2E).

To directly illustrate whether the metabolic effects of adipose-specific Becn1^{F121A} are dependent on elevated adiponectin secretion, we asked whether reduced adiponectin expression abolishes Becn1^{F121A}-induced insulin sensitization in response to HFD feeding, using the *Adiponectin* (*Adipoq*) KO mice. Consistent with previous literature (Nawrocki et al., 2006), we confirmed that the serum adiponectin level in *Adipoq*^{+/-} heterozygous KO mice is approximately half of the WT level after either RD (Figure S7B) or HFD (Figure

S7C) feeding. Thus, we generated heterozygous *Adipoq*^{+/-}; *Adipoq*-Cre/+ mice and then injected them with AAV-Becn1^{F121A} to obtain adipose-specific Becn1^{F121A} mice expressing only one copy of the *Adiponectin* gene. We used AAV-Becn1^{F121A}-injected *Adipoq*^{+/+}; *Adipoq*-Cre/+ mice as the positive control, and AAV-Becn1^{F121A}-injected *Adipoq*^{+/-} KO and WT mice without Cre expression as the negative control. We found that under RD feeding conditions, WT and adipose-Becn1^{F121A} mice expressing both or one copy of *Adiponectin* showed similar body weight, glucose tolerance, and insulin tolerance (Figures S7D and S7E). After HFD feeding, although all four mouse strains had comparable body weight (Figure S7F), only adipose-Becn1^{F121A} mice expressing both copies of *Adiponectin*, but not those expressing just one copy of *Adiponectin*, showed improved glucose tolerance (GTT) and insulin tolerance (ITT) compared with non-Becn1^{F121A}-expressing WT mice (Figure 7C), suggesting that reducing adiponectin in adipose-specific Becn1^{F121A} mice abolishes the systemic insulin-sensitizing effects of adipose Becn1^{F121A} in response to HFD feeding. Indeed, we found that adipose Becn1^{F121A}-induced adiponectin secretion to the circulation is abolished when there is a 50% reduction in adiponectin expression in *Adipoq*^{+/-} mice (Figure 7D). These data further support that the metabolic-improving effects of Becn1^{F121A} are mediated through the adiponectin pathway. Altogether, these findings demonstrate that adipose Becn1 improves systemic glucose tolerance and insulin sensitivity by promoting adiponectin secretion into the circulation.

Model of Becn1-facilitated adiponectin secretion in adipocytes

In addition to the hyperactive genetic mutant Becn1^{F121A}, we found additional upstream physiological and pharmacological modulators of autophagy that also regulate adiponectin secretion. Exercise is a potent physiological inducer of autophagy that disrupts the Becn1-Bcl-2 inhibitory binding (He et al., 2012; Rocchi and He, 2017a). We found that 90-min exercise increases the level of adiponectin in the serum of both male and female WT mice (Figure S7G), suggesting that adiponectin secretion is enhanced by a single bout of exercise. This result is in line with our earlier finding that chronic exercise also increases circulating adiponectin in WT mice, but not in Becn1-inhibited Bcl-2^{AAA} mutant mice (He et al., 2012). This is likely mediated by exercise-induced release of Becn1 from the inhibitory binding of Bcl-2. Via coIP, we found that exercise disrupts the binding of Becn1 with its inhibitor Bcl-2 in the WAT of WT mice (Figure S7H). Although we also detected weak interactions between Becn1 and TLR9 in both WAT and muscle (Figure S7I), different from Becn1-TLR9 binding in muscle, which is enhanced by exercise (Liu et al., 2020), Becn1-TLR9 interaction in the WAT is constitutive and not regulated by exercise (Figure S7I). Thus, we propose that exercise promotes adiponectin secretion by releasing Becn1 from the inhibitory Bcl-2 binding in the WAT.

Conversely, we found that inhibiting the early phase of autophagy imposes an opposite effect. SBI-0206965 and Spautin-1, two inhibitors that block the initiating step of autophagy via inactivating the ULK1 kinase (Egan et al., 2015) or the Vps34 kinase complex (Liu et al., 2011), respectively, reduce the adiponectin level in the serum of WT mice; yet, inhibiting the late stages of autophagy, such as autophagosome-lysosome fusion or autolysosome degradation by chloroquine, does not significantly alter circulating adiponectin levels, measured by WB (Figure 7E) and ELISA analyses (Figure 7F). Given the lack of detection

of adiponectin inside autophagosomes (Figures S4D and S4E), these data support that the upstream PtdIns3K-Becn1 complex, rather than the sequestering and degradative steps of autophagy, is important for adiponectin regulation. Because compared with WT Becn1, Becn1^{F121A} shows reduced binding to its inhibitor Bcl-2 in the WAT (Figure 4A), altogether, we propose the model of Becn1-facilitated adiponectin secretion: under autophagy-inducing conditions that release Becn1 from its inhibitor Bcl-2 (by exercise or the active Becn1^{F121A} mutant), Becn1 interacts with Sec6 and other exocyst components to enhance adiponectin secretion from adipose tissue, which activates AMPK in non-adipose metabolic tissues and systemically increases insulin sensitivity via circulation (Figure 7G).

DISCUSSION

Although emerging evidence suggests that autophagy abnormality is associated with T2D, the mechanism by which autophagy regulates insulin sensitivity is largely unknown. Autophagy is generally thought to be a cellular self-degradation process via lysosomes. In this study, we discovered a previously unknown secretory function regulated by the essential autophagy protein Becn1 in the WAT, which plays a pivotal role in metabolic regulation. We previously found that autophagy-hyperactive Becn1^{F121A} KI mice are protected from HFD-induced insulin resistance (Figure S1A) (Yamamoto et al., 2018). Through analyzing the metabolic signaling pathways in their metabolic tissues, we found that the global Becn1^{F121A} KI mice have higher activation of AMPK, a central player beneficial for energy homeostasis (Figure 1). It is normally believed that autophagy proteins regulate metabolism through cell-autonomous mechanisms, for example, by alleviation of ER stress or improvement of mitochondrial function, because both have been previously linked with insulin sensitization (Patti and Corvera, 2010; Salvadó et al., 2015; Zhang et al., 2013). However, this seems not to be the case in Becn1^{F121A} mice. We found that when added to cell culture media, serum from Becn1^{F121A} mice also enhances AMPK activation in the cells, suggesting that circulating factors are key for Becn1^{F121A}-induced metabolic benefits. To identify the Becn1-regulated, AMPK-activating, circulating factor, we performed a Luminex metabolic hormonal screen in the serum of WT and Becn1^{F121A} mice and detected a higher circulating level of adiponectin in Becn1^{F121A} mice (Figure 2). Adiponectin is a key insulin-sensitizing adipokine that targets multiple metabolic tissues, and its reduction in circulation is strongly associated with T2D and metabolic syndrome. We found that AMPK activation in Becn1^{F121A} mice is at least partially mediated by increased secretion of adiponectin, because the adiponectin receptor of target cells is essential for the AMPK-activating effects of Becn1^{F121A} mouse serum (Figure 3). Based on the findings, we propose that improved insulin sensitivity in Becn1^{F121A} mice is mediated through a non-cell-autonomous mechanism (through the circulating factor adiponectin).

Primary adipocytes from Becn1^{F121A} mice also secrete more adiponectin into medium, suggesting that Becn1^{F121A}-induced adiponectin secretion is cell autonomous. To reveal the underlying mechanism, we carried out a number of different analyses using Becn1^{F121A}-expressing adipocytes. Inhibition of autophagy by disrupting autophagy genes Atg5 or Atg7 in pre-adipocytes impairs normal white adipocyte development and differentiation (Baerga et al., 2009; Singh et al., 2009; Zhang et al., 2009), likely caused by a defect in the removal of organelles (such as mitochondria) during adipogenesis. However, we found that elevating

additional adipokines, how specificity is achieved at the cellular level is worthy of further investigation. The use of different autophagy mutant adipocytes and mouse lines will be useful to understand the role of the autophagy machinery in the regulation of the adipocyte secretome.

Besides the hyperactive *Becn1*^{F121A} genetic mutant, we found that upstream physiological and pharmacological autophagy modulators that alter *Becn1*-*Bcl-2* binding also regulate circulating adiponectin levels. The physiological autophagy inducer exercise and the early-stage autophagy inhibitors have opposite effects on circulating adiponectin. Exercise increases the circulating level of adiponectin (Figure S7G), whereas inhibiting the ULK1 or the *Becn1*-*PtdIns3K* complex (notably not the late-stage autolysosomal degradation) decreases serum adiponectin (Figures 7E and 7F). We propose that autophagy inducers, such as acute and chronic exercise, promotes adiponectin secretion by releasing *Becn1* from inhibitory *Bcl-2* binding in adipose tissue (Figure 7G), rather than through enhancing *Becn1*-TLR9 binding as previously reported in muscle (Liu et al., 2020), for three reasons: (1) via coIP, we found that exercise disrupts the binding of *Becn1* with its inhibitor *Bcl-2* in the WAT of WT mice (Figure S7H); (2) *Becn1*^{F121A} does not change TLR9 levels under either RD or HFD treatment (Figure S1B); and (3) although we detected weak interactions between *Becn1* and TLR9 in both WAT and muscle, different from *Becn1*-TLR9 binding in muscle, which is enhanced by exercise (Liu et al., 2020), *Becn1*-TLR9 interaction in the WAT seems constitutive and not regulated by exercise (Figure S7I). Altogether, our results unveiled a non-degradative, non-cell-autonomous mechanism of *Becn1* in metabolic regulation and demonstrated that *Becn1*-facilitated adiponectin secretion is an important mechanism by which *Becn1* regulates systemic AMPK activity and insulin sensitivity.

STAR★METHODS

RESOURCE AVAILABILITY

Lead contact—Further information and requests for reagents and resources should be directed to and will be fulfilled by the lead contact, Congcong He (congcong.he@northwestern.edu).

Materials availability—The plasmids and mice used in this study are available from the lead contact.

Data and code availability—This study did not generate/analyze datasets/code.

EXPERIMENTAL MODEL AND SUBJECT DETAILS

Animal—All mouse care and procedures were performed in accordance with animal experimental protocols approved by the Northwestern University Institutional Animal Care and Use Committee (IACUC). All mice were housed on a 14-hr/10-hr light/dark cycle with *ad libitum* access to chow diet and water. GFP-LC3 mice, *Becn1*^{F121A} KI mice, and *Becn1*^{+/-} KO mice were described previously (Mizushima et al., 2004; Qu et al., 2003; Rocchi et al., 2017). C57BL/6J mice (JAX#000664), Adiponectin-Cre (Adipoq-Cre) mice (JAX#028020), and Adiponectin KO (Adipoq KO) mice (JAX#008195) were acquired from

the Jackson Laboratory. All strains have been backcrossed for more than 12 generations to C57BL/6J mice. All experiments were performed with sex- and age-matched mice. Diet-induced diabetic mice were generated by HFD (D12492; Research Diets Inc) feeding for 12 weeks. SBI-0206965 (2 mg/kg body weight), Spautin-1 (2 mg/kg body weight) and chloroquine (50 mg/kg body weight) were injected intraperitoneally (i.p.) into mice for 10 consecutive days.

Cell culture—3T3-L1 preadipocytes, HEK293 cells, HEK293FT cells, Flp-In T-REx 293 cells, NIH 3T3 cells, C2C12 myoblasts, HepG2 cells, Huh7 cells, WI-38 cells, GP2–293 cells, and stromal vascular fraction (SVF) cells were cultured in culture medium: Dulbecco's modified Eagle's medium (DMEM) with 10% fetal bovine serum (FBS), 100 units/ml penicillin, and 100 µg/ml streptomycin. For 3T3-L1 preadipocytes differentiation to mature adipocytes, two days after full confluency, 3T3-L1 cells (day 0) were cultured in culture medium supplemented with 0.5 mM IBMX, 1 µM dexamethasone, 1 µg/ml insulin for 2 days. Then cells were cultured in culture medium containing 1 µg/ml insulin and refed every two days. At day 10 of culture, 3T3-L1 adipocytes were utilized for experiments. For C2C12 myoblast differentiation to myotubes, fully confluent C2C12 myoblasts (day 0) were cultured in DMEM containing 2% horse serum, 100 units/ml penicillin and 100 µg/ml streptomycin, and refed with fresh medium every day. At day 6 after differentiation, cells were utilized for experiments.

SVF cells containing fibroblastic preadipocytes were isolated from iWAT of 8 week-old mice by collagenase digestion. Briefly, the iWAT was harvested and washed with ice-cold Hank's balanced salt solution (HBSS). Then iWAT was minced in HBSS containing 300 U/ml type I collagenase and incubated at 37°C for 1 hour with shaking (150 rpm). The digestion was stopped by adding culture medium. The digest was centrifuged at 500 × g for 5 min, and resuspended in the culture medium. After repeating this wash step once again, the cell suspension was filtered through a 70-µm cell strainer and plated in a gelatin-coated dish. To remove non-preadipocytes including red blood cells and immune cells, cells were washed with PBS after 2 hours incubation and then cultured in fresh culture medium. Two days after full confluency, the SVF-derived fibroblastic preadipocytes were cultured in culture medium supplemented with 0.5 mM IBMX, 1 µM dexamethasone, 2 µM rosiglitazone, 1 µg/ml insulin for 2 days. Cells were then cultured in the same way as 3T3-L1 preadipocyte differentiation.

Primary MEFs were isolated from E13.5 embryos by mechanical and enzymatic dissociation method and cultured in MEF culture medium (DMEM with 15% FBS, 2 mM glutamine, 1 x MEM nonessential amino acid, 0.1 mM 2-mercaptoethanol, 100 unit/ml penicillin, and 100 ug/ml streptomycin). Briefly, after the head and red-colored organs were removed from the embryo, tissues were dissociated by pipetting and incubating with 1 mL of 0.05% trypsin-EDTA including 100 kU DNase I (D5025, Millipore Sigma) for 5 min at room temperature. Cell suspension (supernatant) was collected and the digestion was stopped by addition of the MEF culture medium. This digestion step was repeated with the remaining tissues (precipitate). The digest was centrifuged at 300 x g for 5 min and resuspend in the MEF culture medium. The cell suspension was filtered through the 70 µm cell strainer and plated in the culture dish.

Primary hepatocytes were isolated from the adult male mice by perfusing the collagenase solution from the portal vein. Briefly, the mouse was euthanized and perfused with 50 mL of calcium and magnesium ions-free HBSS including 0.5 mM EDTA, followed by 40 mL collagenase solution (HBSS including 200 U/ml type II collagenase [LS004176, Worthington], and 2% BSA) at 5 ml/min using peristaltic pump. After perfusion, the liver was cut into small pieces in the culture medium and passed through the 70 μ m cell strainer. The digest was centrifuged at 40 x g for 2 min and resuspend in the culture medium. To eliminate non-parenchymal cells, dead cells and cell debris, the cell suspension was layered over the 1.077 g/ml Histopaque (10771, Millipore Sigma) and centrifuged at 200 x g for 5 min. Then primary hepatocytes were resuspended in the culture medium and plated in the gelatin-coated dish.

Plasmid—Human Sec6 was cloned from cDNA generated by reverse transcription of the total RNA of WI-38 cells. HA-tagged human SEC6 (HA-hSEC6) and Flag-tagged human BECN1 (Flag-hBECN1) were subcloned into the EcoRI restriction enzyme site of the pcDNA 3.1 (–) vector using In-Fusion cloning kit. Flag-tagged human SEC6 (Flag-hSEC6) and HA-tagged human BECN1 (HA-hBECN1) were subcloned into the EcoRI restriction enzyme site of the pCDH-CMV-MCS-EF1-Puro lentivector using In-Fusion cloning kit. HA-tagged mouse BECN1 (HA-mBECN1) was amplified by PCR from BECLIN-HA WT (Addgene plasmid #46993) (Russell et al., 2013) and ligated into the XbaI and EcoRI restriction enzyme sites of pCDH-CMV-MCS-EF1-Puro lentivector. Flag-hBECN1 mutants and HA-mBECN1 mutants were generated by site-direct mutagenesis. Double-strand oligos encoding shRNAs against the target genes (Table S1) were cloned into pLKO.1-TRC cloning vector lentivector (Addgene plasmid #10878) (Moffat et al., 2006). A scramble shRNA lentivector (Addgene plasmid #1864) (Sarbasov et al., 2005) was used as a negative control.

METHOD DETAILS

AICAR treatment—Prior to the AICAR treatment, cells were incubated in DMEM containing 0.5% FBS for 6 hours. Cells were treated with 1 mM AICAR (10010241, Cayman Chemical) for 2 hours. Then cells were washed with PBS and lysed with hot-Laemmli buffer. The cell lysate was heated at 95°C for 5 min and used for immunoblotting.

GTT and ITT—GTT and ITT were performed as previously described (Yamamoto et al., 2018). Briefly, mice were fasted for 6 hours and 4 hours prior to GTT and ITT, respectively. Glucose was i.p. injected at 1.5 g/kg body weight. Insulin was i.p. injected at 0.75 U/kg in RD-fed mice and 0.5 U/kg in HFD-fed mice. Blood was collected from the tail vein, and the blood glucose levels were measured using glucose meters (Counter Next EZ; Ascensia Diabetes Care). The insulinogenic index was calculated as follows: insulinogenic index = (blood insulin at 15 min - blood insulin at 0 min [picomoles per liter])/(blood glucose at 15 min - blood glucose at 0 min [milligrams per deciliter]).

Hormone ELISA—High molecular weight (HMW) adiponectin levels and total adiponectin levels in mouse serum were determined using ELISA (47-ADPMS-E01, ALPCO; and DY1119, R&D Systems), according to the manufacture's protocol. For serum

insulin measurement, mice were i.p. injected with glucose (1.5 g/kg) after 6 hours of fasting, sera were collected at 0, 15, and 30 min after glucose injection, and serum insulin levels were measured by ELISA (90080; Crystal Chem) according to the manufacture's protocol. Leptin levels in the mouse serum and 3T3-L1 medium were measured by the mouse leptin ELISA kit (DY498-05, R&D Systems). Resistin levels were measured using the resistin ELISA kit (ELM-Resistin, RayBiotech, Inc.). Serum FGF-21 levels were determined using the FGF-21 ELISA kit (KE10042, Proteintech).

Lentivirus production and infection—HEK293FT cells were transfected with a lentiviral expression vector together with a pCMV-VSV-G (Addgene plasmid #8454) (Stewart et al., 2003) and a psPAX2 (Addgene plasmid #12260, a gift from Didier Trono) using the lipofectamine 3000 transfection reagent. Thirty-six hours after transfection, the medium containing the lentivirus was collected and filtered. 3T3-L1 cells, C2C12 cells and NIH 3T3 cells were infected with lentivirus by cell culture in the lentivirus-containing medium with 8 µg/ml polybrene.

Retrovirus production and infection—GP2-293 cells were transfected with pCMV-VSV-G and pBABEpuro GFP-LC3 (Addgene plasmid #22405) (Fung et al., 2008) plasmids using lipofectamine 3000 transfection reagents. Forty-eight hours after transfection, the medium containing the retrovirus was collected and filtered. 3T3-L1 cells were infected with retrovirus by cell culturing in the retrovirus-containing medium with 8 µg/ml polybrene.

Immunopurification of autophagosomes—Autophagosomes were immunopurified from GFP-LC3-expressing 3T3-L1 adipocytes as described previously (Yamamoto et al., 2018). Briefly, cells were homogenized in lysis buffer (0.25 M sucrose, 1 mM EDTA, 20 mM HEPES [pH7.4], 1 x Halt protease and phosphatase inhibitor cocktail) by passing through 27G (5 times) and 30G (10 times) needles. Lysates were centrifuged at 1,000 × g for 10 min at 4°C. The supernatants were recovered and centrifuged at 20,000 × g for 20 min at 4°C. Pellets were resuspended in lysis buffer and incubated with anti-GFP antibody for 2 hours at 4°C. The beads were washed for 4 times with lysis buffer, and the immunoprecipitated proteins were eluted in Laemmli buffer and detected by immunoblotting.

Immunofluorescence staining—Cells were plated on a gelatin-coated cover glass, and were fixed with 4% paraformaldehyde in PBS for 30 min and washed with PBS. The cells were then permeabilized with 0.01% digitonin in PBS for 10 min and incubated with primary antibody in PBS containing 5% normal goat serum. After overnight incubation at 4°C, the cells were washed with PBS and incubated with Alexa Fluor-conjugated secondary antibodies in PBS for 1 hour. After washing with PBS, the cells were mounted in a ProLong Diamond Antifade mountant. Fluorescence images were acquired using a spinning-disk confocal microscope [CSU-W1 spinning disk field scanning confocal system (Yokogawa Electric Corp.) with Hamamatsu Flash 4 camera (Hamamatsu Photonics) mounted to a Nikon Ti2 microscope (Nikon)].

Tandem affinity purification of the Becn1 complex—HEK293 cells stably expressing tetracycline-inducible ZZ tag-hBECN1-3 × Flag were generated using the

pZZ-3XFlag construct (Sun et al., 2008) and the Flp-In T-REx 293 cell system according to the manufacturer's protocol. Cells were incubated in culture medium containing 1 µg/ml tetracycline for 24 hours. After washing with PBS, the cells were lysed in Triton X-100 cell lysis buffer. The lysate was centrifuged at $15,000 \times g$ for 10 min at 4°C, and the supernatant was incubated with IgG Sepharose for 3 hours at 4°C. The bound proteins were then eluted by TEV protease cleavage. The eluate was incubated with anti-Flag antibody-conjugated beads for 14–16 hours at 4°C, and the bound proteins were eluted in Laemmli buffer and detected by immunoblotting.

Co-immunoprecipitation (co-IP)—HEK293 cells transfected with plasmids by the lipofectamine 3000 transfection reagent, SVF-derived adipocytes, or mouse WAT and muscle were lysed in Triton X-100 cell lysis buffer (1% Triton X-100, 20 mM HEPES [pH7.4], 150 mM NaCl, 1 mM EDTA). The lysate was centrifuged at $15,000 \times g$ for 10 min at 4°C, the supernatant was incubated with the target protein-specific antibody and Protein A/G beads for 14–16 hours at 4°C. After bead washing for 4 times with Triton X-100 cell lysis buffer, immunoprecipitated proteins were eluted in Laemmli buffer and detected by immunoblotting.

AAV delivery of pAAV-FLEX-3xFlag-mBecn1^{F121A}—The EGFP ORF region of the pAAV-FLEX-GFP plasmid (Addgene plasmid #28304, a gift from Edward Boyden) was replaced by 3xFlag-mBecn1^{F121A} ORF using KpnI and XhoI restriction enzymes (NEB) and the In-Fusion HD Plus cloning kit. The AAV2/8 virus was produced by the Sanford Burnham Prebys Medical Discovery Institute Viral Vector Core Facility. The virus titer was 9×10^{12} (virus genome (VG)/ml). Viral aliquots were stored at -80°C until injection.

6-week old mice were anesthetized with ketamine (100 mg/kg body weight) and xylazine (10 mg/kg body weight). Hairs were removed from the iWAT area using clippers and hair depilatory cream. The surgical area was disinfected with 5% povidone-iodine solution followed by 70% ethanol. A small incision was made on the skin using surgical scissors, and exposed the iWAT. 5×10^{10} VG per 30 µl phosphate-buffered saline (PBS) virus solution was injected into each iWAT lobe using a 31 G insulin syringe (BD). The skin was closed with an absorbable suture. For gWAT delivery, 5×10^{10} VG per 100 µl PBS virus solution was i.p. injected into the gWAT of the same mouse. For postoperative care, mice were injected subcutaneously with meloxicam (0.5 mg/kg body weight) for two consecutive days.

Total lipid extraction and TG measurement—Total lipids were extracted from the mouse liver using the Bligh and Dyer method (Bligh and Dyer, 1959). Extracted total lipids were resuspended in isopropanol. TG levels were measured using Infinity Triglycerides Liquid Stable Reagent (TR22421, Thermo Fisher Scientific) according to the manufacturer's protocol.

Treadmill exercise—Exercise was performed as described previously (He et al., 2012) using a 10° uphill Exer 3/6 open treadmill (Columbus Instruments), with some modifications. Briefly, for acclimation, on day 1, mice ran for 5 min at 8 m/min, and on day 2, mice ran for 5 min at 8 m/min followed by another 5 min at 10 m/min. On day 3, mice were subject to running exercise starting at 12 m/min for 40 min. After 40 min, the treadmill

speed was increased at the rate of 1 m/min every 10 min for 30 min and then every 5 min for 20 min.

RT-PCR and qPCR—Total RNA was isolated from the 3T3-L1 adipocytes and the mouse liver using the Trizol Reagent. Two micrograms of total RNA was reverse-transcribed using High-Capacity cDNA Reverse Transcription kit (4368814, Thermo Fisher Scientific) according to the manufacturer's protocol. RT-PCR (reverse transcription-PCR) was performed using SapphireAmp Fast PCR Master Mix (RR350, Takara Bio Inc.). The amplicons were separated and detected by agarose gel electrophoresis and ethidium bromide staining. The band intensity was measured using ImageJ software. qPCR (quantitative PCR) was performed using the PowerUP SYBR Green Master Mix and QuantStudio 7 Flex Real-Time PCR system (Thermo Fisher Scientific). The relative gene expressions were quantified using the $-2^{\Delta\Delta Ct}$ method and normalized to *Actb*. The sequences of the primers used for PCR are listed in Table S2.

Immunoblotting—For Akt phosphorylation in the liver, mice were i.p. injected with insulin (1.5 U/kg) after 4 hours fasting, and tissues were collected 15 minutes after insulin injection. For all immunoblotting analyses, tissues and cells were lysed using RIPA lysis buffer (20 mM Tris-HCl [pH 7.4], 150 mM NaCl, 1% NP-40, 0.1% sodium lauryl sulfate [SDS], 0.5% sodium deoxycholate, 1 mM EDTA, 1 x Halt protease and phosphatase inhibitor cocktail). After centrifugation at $15,000 \times g$ for 10 min at 4°C, the supernatant was collected and protein concentration was determined using a BCA protein assay kit. Proteins were denatured in Laemmli buffer by heating at 95°C for 5 min. Samples containing the equivalent amount of protein were resolved by SDS-PAGE and transferred to polyvinylidene difluoride (PVDF) membrane or nitrocellulose membrane. After membrane blocking by 0.5% skim milk in Tris-buffered saline containing 0.05% Tween-20 (TBS-T), the proteins were probed with primary antibody overnight at 4°C. The membrane was then washed with TBS-T for 10 min 3 times, and incubated with HRP-conjugated secondary antibody for 1 hour. After membrane washing with TBS-T, specific bands were visualized by chemiluminescence and myECL imager (Thermo Fisher Scientific). The band intensities were quantified using ImageJ software.

QUANTIFICATION AND STATISTICAL ANALYSIS

All data are shown as mean \pm standard errors of the mean (SEM). Data were analyzed by Student's t test for two groups, and by one-way analysis of variance (ANOVA) followed by Tukey-Kramer test or Dunnett's test for more than two groups. The difference with a P value of < 0.05 was considered statistically significant. Please note that statistical details are found in the figure legends.

Supplementary Material

Refer to Web version on PubMed Central for supplementary material.

ACKNOWLEDGMENTS

We thank Dr. Qing Zhong for providing the pZZ-FLAG construct; Dr. Noboru Mizushima for providing the GFP-LC3 mice; Sanford Burnham Prebys Medical Discovery Institute Viral Vector Core Facility for AAV production; and the following facilities at Northwestern University Feinberg School of Medicine for technical support: the Comprehensive Metabolic Core for metabolic hormone multiplex analyses, the Center for Advanced Microscopy for confocal microscopy studies, the NUSeq Core of Center for Genetic Medicine for qPCR analyses, and the Sanger Sequencing Core for sequencing. The study is supported by NIH R01-DK113170 and Northwestern University Lurie Cancer Center Translational Bridge Award (to C.H.).

REFERENCES

- Arita Y, Kihara S, Ouchi N, Takahashi M, Maeda K, Miyagawa J, Hotta K, Shimomura I, Nakamura T, Miyaoka K, et al. (1999). Paradoxical decrease of an adipose-specific protein, adiponectin, in obesity. *Biochem. Biophys. Res. Commun* 257, 79–83. [PubMed: 10092513]
- Baerga R, Zhang Y, Chen PH, Goldman S, and Jin S (2009). Targeted deletion of autophagy-related 5 (atg5) impairs adipogenesis in a cellular model and in mice. *Autophagy* 5, 1118–1130. [PubMed: 19844159]
- Basu R, Pajvani UB, Rizza RA, and Scherer PE (2007). Selective downregulation of the high molecular weight form of adiponectin in hyperinsulinemia and in type 2 diabetes: differential regulation from nondiabetic subjects. *Diabetes* 56, 2174–2177. [PubMed: 17513700]
- Bel S, Pendse M, Wang Y, Li Y, Ruhn KA, Hassell B, Leal T, Winter SE, Xavier RJ, and Hooper LV (2017). Paneth cells secrete lysozyme via secretory autophagy during bacterial infection of the intestine. *Science* 357, 1047–1052. [PubMed: 28751470]
- Bligh EG, and Dyer WJ (1959). A rapid method of total lipid extraction and purification. *Can. J. Biochem. Physiol* 37, 911–917. [PubMed: 13671378]
- Blüher RM, van Roomen CP, Meijer AJ, Houben-Weerts JH, Sauerwein HP, and Dubbelhuis PF (2008). Regulation of adiponectin secretion by insulin and amino acids in 3T3-L1 adipocytes. *Metabolism* 57, 1655–1662. [PubMed: 19013287]
- Bodemann BO, Orvedahl A, Cheng T, Ram RR, Ou YH, Formstecher E, Maiti M, Hazelett CC, Wauson EM, Balakireva M, et al. (2011). RalB and the exocyst mediate the cellular starvation response by direct activation of autophagosome assembly. *Cell* 144, 253–267. [PubMed: 21241894]
- Cong L, Chen K, Li J, Gao P, Li Q, Mi S, Wu X, and Zhao AZ (2007). Regulation of adiponectin and leptin secretion and expression by insulin through a PI3K-PDE3B dependent mechanism in rat primary adipocytes. *Biochem. J* 403, 519–525. [PubMed: 17286556]
- Ebato C, Uchida T, Arakawa M, Komatsu M, Ueno T, Komiya K, Azuma K, Hirose T, Tanaka K, Kominami E, et al. (2008). Autophagy is important in islet homeostasis and compensatory increase of beta cell mass in response to high-fat diet. *Cell Metab.* 8, 325–332. [PubMed: 18840363]
- Egan DF, Chun MG, Vamos M, Zou H, Rong J, Miller CJ, Lou HJ, Raveendra-Panickar D, Yang CC, Sheffler DJ, et al. (2015). Small Molecule Inhibition of the Autophagy Kinase ULK1 and Identification of ULK1 Substrates. *Mol. Cell* 59, 285–297. [PubMed: 26118643]
- Fung C, Lock R, Gao S, Salas E, and Debnath J (2008). Induction of autophagy during extracellular matrix detachment promotes cell survival. *Mol. Biol. Cell* 19, 797–806. [PubMed: 18094039]
- Garcia D, and Shaw RJ (2017). AMPK: Mechanisms of Cellular Energy Sensing and Restoration of Metabolic Balance. *Mol. Cell* 66, 789–800. [PubMed: 28622524]
- Geng L, Liao B, Jin L, Huang Z, Triggler CR, Ding H, Zhang J, Huang Y, Lin Z, and Xu A (2019). Exercise Alleviates Obesity-Induced Metabolic Dysfunction via Enhancing FGF21 Sensitivity in Adipose Tissues. *Cell Rep.* 26, 2738–2752.e4. [PubMed: 30840894]
- Gwinn DM, Shackelford DB, Egan DF, Mihaylova MM, Mery A, Vasquez DS, Turk BE, and Shaw RJ (2008). AMPK phosphorylation of raptor mediates a metabolic checkpoint. *Mol. Cell* 30, 214–226. [PubMed: 18439900]
- Haemmerle G, Moustafa T, Woelkart G, Büttner S, Schmidt A, van de Weijer T, Hesselink M, Jaeger D, Kienesberger PC, Zierler K, et al. (2011). ATGL-mediated fat catabolism regulates cardiac mitochondrial function via PPAR- α and PGC-1. *Nat. Med* 17, 1076–1085. [PubMed: 21857651]

- Hajri T, Tao H, Wattacheril J, Marks-Shulman P, and Abumrad NN (2011). Regulation of adiponectin production by insulin: interactions with tumor necrosis factor- α and interleukin-6. *Am. J. Physiol. Endocrinol. Metab.* 300, E350–E360. [PubMed: 21062957]
- Hara K, Boutin P, Mori Y, Tobe K, Dina C, Yasuda K, Yamauchi T, Otabe S, Okada T, Eto K, et al. (2002). Genetic variation in the gene encoding adiponectin is associated with an increased risk of type 2 diabetes in the Japanese population. *Diabetes* 51, 536–540. [PubMed: 11812766]
- Haruta T, Uno T, Kawahara J, Takano A, Egawa K, Sharma PM, Olefsky JM, and Kobayashi M (2000). A rapamycin-sensitive pathway downregulates insulin signaling via phosphorylation and proteasomal degradation of insulin receptor substrate-1. *Mol. Endocrinol* 14, 783–794. [PubMed: 10847581]
- He C, and Levine B (2010). The Beclin 1 interactome. *Curr. Opin. Cell Biol* 22, 140–149. [PubMed: 20097051]
- He C, Bassik MC, Moresi V, Sun K, Wei Y, Zou Z, An Z, Loh J, Fisher J, Sun Q, et al. (2012). Exercise-induced BCL2-regulated autophagy is required for muscle glucose homeostasis. *Nature* 481, 511–515. [PubMed: 22258505]
- He C, Wei Y, Sun K, Li B, Dong X, Zou Z, Liu Y, Kinch LN, Khan S, Sinha S, et al. (2013). Beclin 2 functions in autophagy, degradation of G protein-coupled receptors, and metabolism. *Cell* 154, 1085–1099. [PubMed: 23954414]
- Heider MR, and Munson M (2012). Exorcising the exocyst complex. *Traffic* 13, 898–907. [PubMed: 22420621]
- Holland WL, Miller RA, Wang ZV, Sun K, Barth BM, Bui HH, Davis KE, Bikman BT, Halberg N, Rutkowski JM, et al. (2011). Receptor-mediated activation of ceramidase activity initiates the pleiotropic actions of adiponectin. *Nat. Med* 17, 55–63. [PubMed: 21186369]
- Holland WL, Adams AC, Brozinick JT, Bui HH, Miyauchi Y, Kusminski CM, Bauer SM, Wade M, Singhal E, Cheng CC, et al. (2013). An FGF21-adiponectin-ceramide axis controls energy expenditure and insulin action in mice. *Cell Metab.* 17, 790–797. [PubMed: 23663742]
- Hotta K, Funahashi T, Bodkin NL, Ortmeier HK, Arita Y, Hansen BC, and Matsuzawa Y (2001). Circulating concentrations of the adipocyte protein adiponectin are decreased in parallel with reduced insulin sensitivity during the progression to type 2 diabetes in rhesus monkeys. *Diabetes* 50, 1126–1133. [PubMed: 11334417]
- Jimenez V, Muñoz S, Casana E, Mallol C, Elias I, Jambrina C, Ribera A, Ferre T, Franckhauser S, and Bosch F (2013). In vivo adeno-associated viral vector-mediated genetic engineering of white and brown adipose tissue in adult mice. *Diabetes* 62, 4012–4022. [PubMed: 24043756]
- Jung HS, Chung KW, Won Kim J, Kim J, Komatsu M, Tanaka K, Nguyen YH, Kang TM, Yoon KH, Kim JW, et al. (2008). Loss of autophagy diminishes pancreatic beta cell mass and function with resultant hyperglycemia. *Cell Metab.* 8, 318–324. [PubMed: 18840362]
- Kadowaki T, Yamauchi T, Kubota N, Hara K, Ueki K, and Tobe K (2006). Adiponectin and adiponectin receptors in insulin resistance, diabetes, and the metabolic syndrome. *J. Clin. Invest* 116, 1784–1792. [PubMed: 16823476]
- Kaur J, and Debnath J (2015). Autophagy at the crossroads of catabolism and anabolism. *Nat. Rev. Mol. Cell Biol.* 16, 461–472. [PubMed: 26177004]
- Komai AM, Musovic S, Peris E, Alrifaiy A, El Hachmane MF, Johansson M, Wernstedt Asterholm I, and Olofsson CS (2016). White Adipocyte Adiponectin Exocytosis Is Stimulated via β_3 -Adrenergic Signaling and Activation of Epac1: Catecholamine Resistance in Obesity and Type 2 Diabetes. *Diabetes* 65, 3301–3313. [PubMed: 27554468]
- Kondo H, Shimomura I, Matsukawa Y, Kumada M, Takahashi M, Matsuda M, Ouchi N, Kihara S, Kawamoto T, Sumitsuji S, et al. (2002). Association of adiponectin mutation with type 2 diabetes: a candidate gene for the insulin resistance syndrome. *Diabetes* 51, 2325–2328. [PubMed: 12086969]
- Kubota N, Terauchi Y, Yamauchi T, Kubota T, Moroi M, Matsui J, Eto K, Yamashita T, Kamon J, Satoh H, et al. (2002). Disruption of adiponectin causes insulin resistance and neointimal formation. *J. Biol. Chem* 277, 25863–25866. [PubMed: 12032136]
- Kuramoto K, and He C (2018). The BECN1-BCL2 complex regulates insulin secretion and storage in mice. *Autophagy* 14, 2026–2028. [PubMed: 30081744]

- Lara-Castro C, Luo N, Wallace P, Klein RL, and Garvey WT (2006). Adiponectin multimeric complexes and the metabolic syndrome trait cluster. *Diabetes* 55, 249–259. [PubMed: 16380500]
- Leidal AM, Huang HH, Marsh T, Solvik T, Zhang D, Ye J, Kai F, Goldsmith J, Liu JY, Huang YH, et al. (2020). The LC3-conjugation machinery specifies the loading of RNA-binding proteins into extracellular vesicles. *Nat. Cell Biol.* 22, 187–199. [PubMed: 31932738]
- Levine B, Liu R, Dong X, and Zhong Q (2015). Beclin orthologs: integrative hubs of cell signaling, membrane trafficking, and physiology. *Trends Cell Biol.* 25, 533–544. [PubMed: 26071895]
- Li S, Shin HJ, Ding EL, and van Dam RM (2009). Adiponectin levels and risk of type 2 diabetes: a systematic review and meta-analysis. *JAMA* 302, 179–188. [PubMed: 19584347]
- Li Y, Xu S, Mihaylova MM, Zheng B, Hou X, Jiang B, Park O, Luo Z, Lefai E, Shyy JY, et al. (2011). AMPK phosphorylates and inhibits SREBP activity to attenuate hepatic steatosis and atherosclerosis in diet-induced insulin-resistant mice. *Cell Metab.* 13, 376–388. [PubMed: 21459323]
- Lim CY, Hong W, and Han W (2015). Adiponectin is released via a unique regulated exocytosis pathway from a pre-formed vesicle pool on insulin stimulation. *Biochem. J* 471, 381–389. [PubMed: 26330614]
- Lin Z, Tian H, Lam KS, Lin S, Hoo RC, Konishi M, Itoh N, Wang Y, Bornstein SR, Xu A, and Li X (2013). Adiponectin mediates the metabolic effects of FGF21 on glucose homeostasis and insulin sensitivity in mice. *Cell Metab.* 17, 779–789. [PubMed: 23663741]
- Liu J, Xia H, Kim M, Xu L, Li Y, Zhang L, Cai Y, Norberg HV, Zhang T, Furuya T, et al. (2011). Beclin1 controls the levels of p53 by regulating the deubiquitination activity of USP10 and USP13. *Cell* 147, 223–234. [PubMed: 21962518]
- Liu Y, Nguyen PT, Wang X, Zhao Y, Meacham CE, Zou Z, Bordieanu B, Johanns M, Vertommen D, Wijshake T, et al. (2020). TLR9 and beclin 1 crosstalk regulates muscle AMPK activation in exercise. *Nature* 578, 605–609. [PubMed: 32051584]
- Masuda Y, Itabe H, Odaki M, Hama K, Fujimoto Y, Mori M, Sasabe N, Aoki J, Arai H, and Takano T (2006). ADRP/adipophilin is degraded through the proteasome-dependent pathway during regression of lipid-storing cells. *J. Lipid Res.* 47, 87–98. [PubMed: 16230742]
- Mei K, Li Y, Wang S, Shao G, Wang J, Ding Y, Luo G, Yue P, Liu JJ, Wang X, et al. (2018). Cryo-EM structure of the exocyst complex. *Nat. Struct. Mol. Biol* 25, 139–146. [PubMed: 29335562]
- Menzaghi C, Ercolino T, Di Paola R, Berg AH, Warram JH, Scherer PE, Trischitta V, and Doria A (2002). A haplotype at the adiponectin locus is associated with obesity and other features of the insulin resistance syndrome. *Diabetes* 51, 2306–2312. [PubMed: 12086965]
- Mizushima N, Yamamoto A, Matsui M, Yoshimori T, and Ohsumi Y (2004). In vivo analysis of autophagy in response to nutrient starvation using transgenic mice expressing a fluorescent autophagosome marker. *Mol. Biol. Cell* 15, 1101–1111. [PubMed: 14699058]
- Moffat J, Grueneberg DA, Yang X, Kim SY, Kloepfer AM, Hinkle G, Piqani B, Eisenhaure TM, Luo B, Grenier JK, et al. (2006). A lentiviral RNAi library for human and mouse genes applied to an arrayed viral high-content screen. *Cell* 124, 1283–1298. [PubMed: 16564017]
- Murdolo G, Hammarstedt A, Schmelz M, Jansson PA, and Smith U (2009). Acute hyperinsulinemia differentially regulates interstitial and circulating adiponectin oligomeric pattern in lean and insulin-resistant, obese individuals. *J. Clin. Endocrinol. Metab* 94, 4508–4516. [PubMed: 19820029]
- Murthy M, Garza D, Scheller RH, and Schwarz TL (2003). Mutations in the exocyst component Sec5 disrupt neuronal membrane traffic, but neurotransmitter release persists. *Neuron* 37, 433–447. [PubMed: 12575951]
- Nawrocki AR, Rajala MW, Tomas E, Pajvani UB, Saha AK, Trumbauer ME, Pang Z, Chen AS, Ruderman NB, Chen H, et al. (2006). Mice lacking adiponectin show decreased hepatic insulin sensitivity and reduced responsiveness to peroxisome proliferator-activated receptor gamma agonists. *J. Biol. Chem* 281, 2654–2660. [PubMed: 16326714]
- Ouchi N, Parker JL, Lugus JJ, and Walsh K (2011). Adipokines in inflammation and metabolic disease. *Nat. Rev. Immunol* 11, 85–97. [PubMed: 21252989]
- Ozes ON, Akca H, Mayo LD, Gustin JA, Maehama T, Dixon JE, and Donner DB (2001). A phosphatidylinositol 3-kinase/Akt/mTOR pathway mediates and PTEN antagonizes tumor necrosis

- factor inhibition of insulin signaling through insulin receptor substrate-1. *Proc. Natl. Acad. Sci. USA* 98, 4640–4645. [PubMed: 11287630]
- Pajvani UB, Hawkins M, Combs TP, Rajala MW, Doebber T, Berger JP, Wagner JA, Wu M, Knopps A, Xiang AH, et al. (2004). Complex distribution, not absolute amount of adiponectin, correlates with thiazolidinedione-mediated improvement in insulin sensitivity. *J. Biol. Chem* 279, 12152–12162. [PubMed: 14699128]
- Patti ME, and Corvera S (2010). The role of mitochondria in the pathogenesis of type 2 diabetes. *Endocr. Rev* 31, 364–395. [PubMed: 20156986]
- Pederson TM, Kramer DL, and Rondinone CM (2001). Serine/threonine phosphorylation of IRS-1 triggers its degradation: possible regulation by tyrosine phosphorylation. *Diabetes* 50, 24–31. [PubMed: 11147790]
- Qu X, Yu J, Bhagat G, Furuya N, Hibshoosh H, Troxel A, Rosen J, Eskelinen EL, Mizushima N, Ohsumi Y, et al. (2003). Promotion of tumorigenesis by heterozygous disruption of the beclin 1 autophagy gene. *J. Clin. Invest* 112, 1809–1820. [PubMed: 14638851]
- Rakhshandehroo M, Knoch B, Müller M, and Kersten S (2010). Peroxisome proliferator-activated receptor alpha target genes. *PPAR Res.* 2010, 612089. [PubMed: 20936127]
- Rocchi A, and He C (2015). Emerging roles of autophagy in metabolism and metabolic disorders. *Front. Biol. (Beijing)* 10, 154–164. [PubMed: 26989402]
- Rocchi A, and He C (2017a). Activating Autophagy by Aerobic Exercise in Mice. *J. Vis. Exp.* 2017, 55099.
- Rocchi A, and He C (2017b). Regulation of Exercise-Induced Autophagy in Skeletal Muscle. *Curr. Pathobiol. Rep* 5, 177–186. [PubMed: 29057166]
- Rocchi A, Yamamoto S, Ting T, Fan Y, Sadleir K, Wang Y, Zhang W, Huang S, Levine B, Vassar R, and He C (2017). A *Becn1* mutation mediates hyperactive autophagic sequestration of amyloid oligomers and improved cognition in Alzheimer's disease. *PLoS Genet.* 13, e1006962. [PubMed: 28806762]
- Russell RC, Tian Y, Yuan H, Park HW, Chang YY, Kim J, Kim H, Neufeld TP, Dillin A, and Guan KL (2013). ULK1 induces autophagy by phosphorylating Beclin-1 and activating VPS34 lipid kinase. *Nat. Cell Biol.* 15, 741–750. [PubMed: 23685627]
- Salvadó L, Palomer X, Barroso E, and Vázquez-Carrera M (2015). Targeting endoplasmic reticulum stress in insulin resistance. *Trends Endocrinol. Metab.* 26, 438–448. [PubMed: 26078196]
- Sarbassov DD, Guertin DA, Ali SM, and Sabatini DM (2005). Phosphorylation and regulation of Akt/PKB by the rictor-mTOR complex. *Science* 307, 1098–1101. [PubMed: 15718470]
- Singh R, Xiang Y, Wang Y, Baikati K, Cuervo AM, Luu YK, Tang Y, Pessin JE, Schwartz GJ, and Czaja MJ (2009). Autophagy regulates adipose mass and differentiation in mice. *J. Clin. Invest* 119, 3329–3339. [PubMed: 19855132]
- Stern JH, Rutkowski JM, and Scherer PE (2016). Adiponectin, Leptin, and Fatty Acids in the Maintenance of Metabolic Homeostasis through Adipose Tissue Crosstalk. *Cell Metab.* 23, 770–784. [PubMed: 27166942]
- Stewart SA, Dykxhoorn DM, Palliser D, Mizuno H, Yu EY, An DS, Sabatini DM, Chen IS, Hahn WC, Sharp PA, et al. (2003). Lentivirus-delivered stable gene silencing by RNAi in primary cells. *RNA* 9, 493–501. [PubMed: 12649500]
- Stumvoll M, Tschrirter O, Fritsche A, Staiger H, Renn W, Weisser M, Machicao F, and Häring H (2002). Association of the T-G polymorphism in adiponectin (exon 2) with obesity and insulin sensitivity: interaction with family history of type 2 diabetes. *Diabetes* 51, 37–41. [PubMed: 11756320]
- Sun XJ, Goldberg JL, Qiao LY, and Mitchell JJ (1999). Insulin-induced insulin receptor substrate-1 degradation is mediated by the proteasome degradation pathway. *Diabetes* 48, 1359–1364. [PubMed: 10389839]
- Sun Q, Fan W, Chen K, Ding X, Chen S, and Zhong Q (2008). Identification of Barkor as a mammalian autophagy-specific factor for Beclin 1 and class III phosphatidylinositol 3-kinase. *Proc. Natl. Acad. Sci. USA* 105, 19211–19216. [PubMed: 19050071]
- Takano A, Usui I, Haruta T, Kawahara J, Uno T, Iwata M, and Kobayashi M (2001). Mammalian target of rapamycin pathway regulates insulin signaling via subcellular redistribution of insulin receptor

- substrate 1 and integrates nutritional signals and metabolic signals of insulin. *Mol. Cell. Biol* 21, 5050–5062. [PubMed: 11438661]
- Ueno M, Carvalheira JB, Tambascia RC, Bezerra RM, Amaral ME, Carneiro EM, Folli F, Franchini KG, and Saad MJ (2005). Regulation of insulin signalling by hyperinsulinaemia: role of IRS-1/2 serine phosphorylation and the mTOR/p70 S6K pathway. *Diabetologia* 48, 506–518. [PubMed: 15692808]
- Werner ED, Lee J, Hansen L, Yuan M, and Shoelson SE (2004). Insulin resistance due to phosphorylation of insulin receptor substrate-1 at serine 302. *J. Biol. Chem* 279, 35298–35305. [PubMed: 15199052]
- Wu B, and Guo W (2015). The Exocyst at a Glance. *J. Cell Sci* 128, 2957–2964. [PubMed: 26240175]
- Wu X, Motoshima H, Mahadev K, Stalker TJ, Scalia R, and Goldstein BJ (2003). Involvement of AMP-activated protein kinase in glucose uptake stimulated by the globular domain of adiponectin in primary rat adipocytes. *Diabetes* 52, 1355–1363. [PubMed: 12765944]
- Xie L, O'Reilly CP, Chapes SK, and Mora S (2008). Adiponectin and leptin are secreted through distinct trafficking pathways in adipocytes. *Biochim. Biophys. Acta* 1782, 99–108. [PubMed: 18179777]
- Xu G, Sztalryd C, Lu X, Tansey JT, Gan J, Dorward H, Kimmel AR, and Londos C (2005). Post-translational regulation of adipose differentiation-related protein by the ubiquitin/proteasome pathway. *J. Biol. Chem* 280, 42841–42847. [PubMed: 16115879]
- Yamamoto S, Kuramoto K, Wang N, Situ X, Priyadarshini M, Zhang W, Cordoba-Chacon J, Layden BT, and He C (2018). Autophagy Differentially Regulates Insulin Production and Insulin Sensitivity. *Cell Rep.* 23, 3286–3299. [PubMed: 29898399]
- Yamauchi T, Kamon J, Waki H, Terauchi Y, Kubota N, Hara K, Mori Y, Ide T, Murakami K, Tsuboyama-Kasaoka N, et al. (2001). The fat-derived hormone adiponectin reverses insulin resistance associated with both lipoatrophy and obesity. *Nat. Med* 7, 941–946. [PubMed: 11479627]
- Yamauchi T, Kamon J, Minokoshi Y, Ito Y, Waki H, Uchida S, Yamashita S, Noda M, Kita S, Ueki K, et al. (2002). Adiponectin stimulates glucose utilization and fatty-acid oxidation by activating AMP-activated protein kinase. *Nat. Med* 8, 1288–1295. [PubMed: 12368907]
- Yang L, Li P, Fu S, Calay ES, and Hotamisligil GS (2010). Defective hepatic autophagy in obesity promotes ER stress and causes insulin resistance. *Cell Metab.* 11, 467–478. [PubMed: 20519119]
- Yoon MJ, Lee GY, Chung JJ, Ahn YH, Hong SH, and Kim JB (2006). Adiponectin increases fatty acid oxidation in skeletal muscle cells by sequential activation of AMP-activated protein kinase, p38 mitogen-activated protein kinase, and peroxisome proliferator-activated receptor alpha. *Diabetes* 55, 2562–2570. [PubMed: 16936205]
- Zhang Y, Goldman S, Baerga R, Zhao Y, Komatsu M, and Jin S (2009). Adipose-specific deletion of autophagy-related gene 7 (*atg7*) in mice reveals a role in adipogenesis. *Proc. Natl. Acad. Sci. USA* 106, 19860–19865. [PubMed: 19910529]
- Zhang W, Hietakangas V, Wee S, Lim SC, Gunaratne J, and Cohen SM (2013). ER stress potentiates insulin resistance through PERK-mediated FOXO phosphorylation. *Genes Dev.* 27, 441–449. [PubMed: 23431056]
- Zhang M, Kenny SJ, Ge L, Xu K, and Schekman R (2015). Translocation of interleukin-1b into a vesicle intermediate in autophagy-mediated secretion. *eLife* 4, e11205. [PubMed: 26523392]

Highlights

- Autophagy-hyperactive *Becn1*^{F121A} mice show systemic activation of AMPK
- *Becn1* positively regulates the secretion of an adipokine, adiponectin
- *Becn1*-exocyst interaction is essential for facilitating adiponectin secretion
- Adipose *Becn1*^{F121A} is sufficient to improve metabolism by elevating serum adiponectin

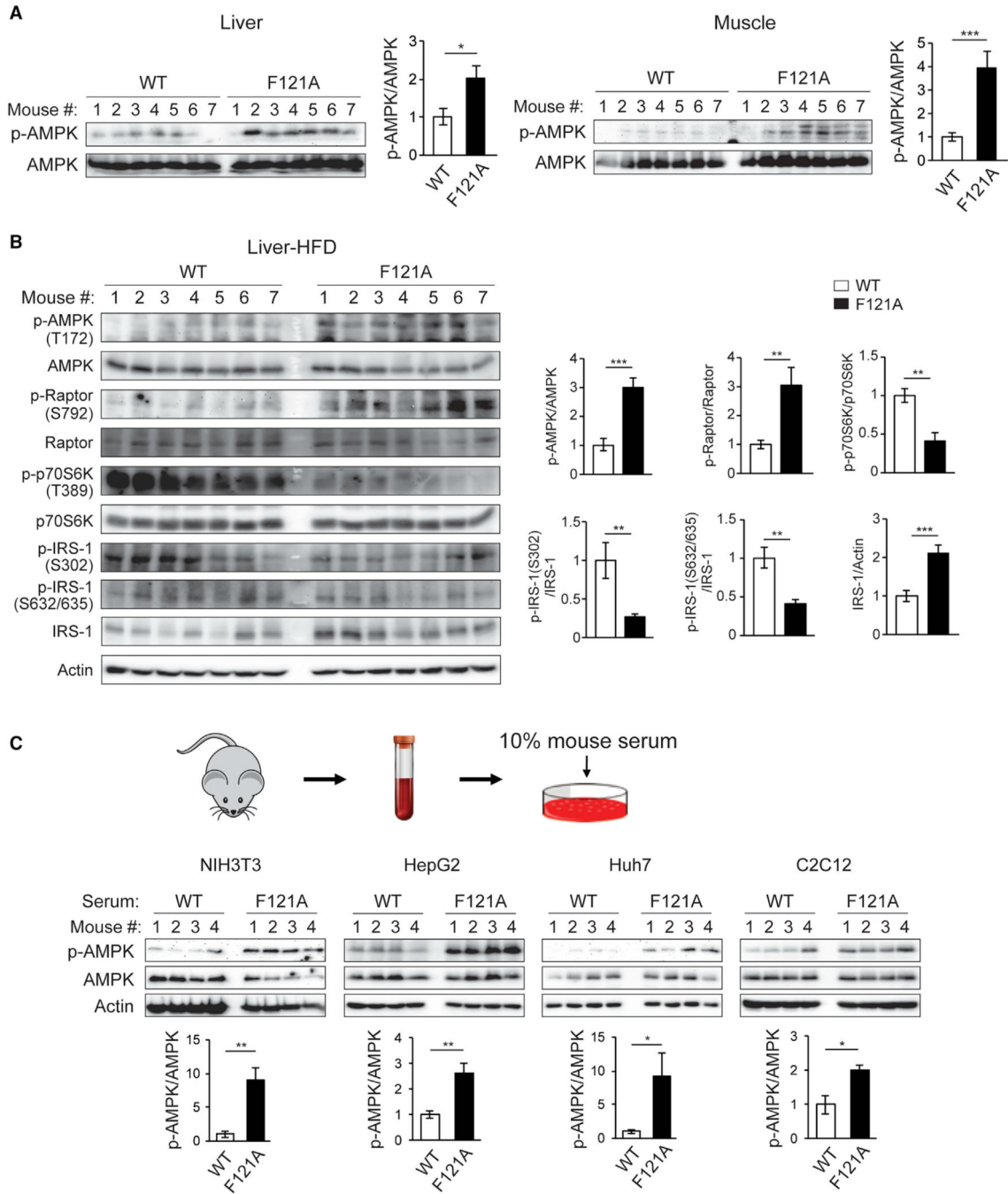


Figure 1. Autophagy-hyperactive *Becn1*^{F121A} mice show enhanced AMPK activation in tissues, caused by factors in circulation

(A) Metabolic tissues of *Becn1*^{F121A} KI mice show increased AMPK activation. Western blot (WB) analysis and quantification of AMPK phosphorylation in liver and muscle of *Becn1*^{F121A} mice. n = 7.

(B) WB analysis and quantification of AMPK activation and signaling pathways downstream of AMPK in the liver of HFD-fed WT and *Becn1*^{F121A} mice. n = 7.

(C) Circulating factors in *Becn1*^{F121A} mice play a role in activating AMPK. WB analysis of AMPK phosphorylation in cell lines cultured for 1 h in medium containing 10% mouse serum from WT or *Becn1*^{F121A} mice. n = 4.

Data represent mean \pm SEM, t test. *p < 0.05; **p < 0.01; ***p < 0.001.

Author Manuscript

Author Manuscript

Author Manuscript

Author Manuscript

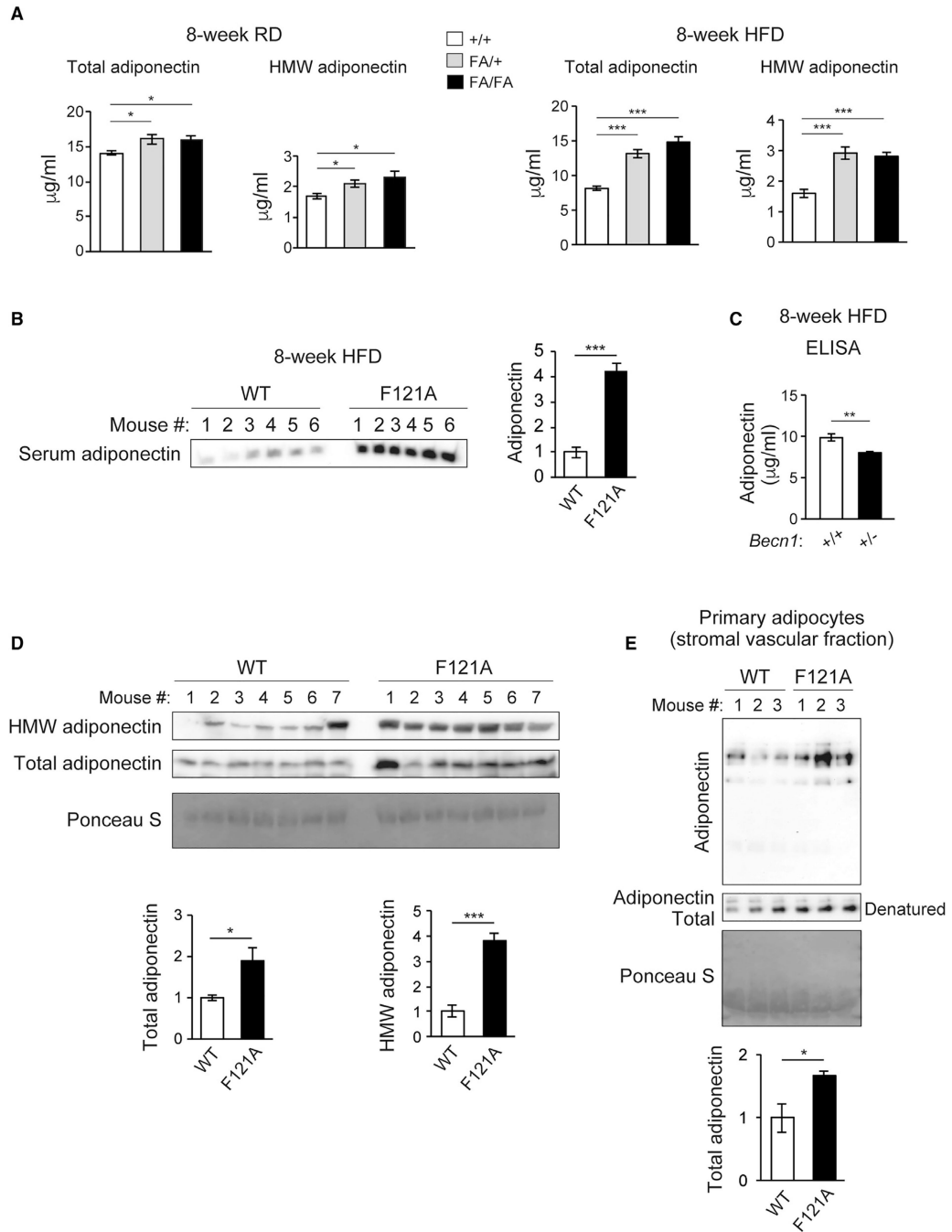


Figure 2. Becl1 positively regulates adiponectin secretion *in vivo* and *in vitro*

(A) ELISA of total adiponectin and HMW adiponectin in the serum of WT (+/+) mice and heterozygous (FA/+) or homozygous (FA/FA) *Becl1*^{F121A} KI mice fed with RD (regular diet) or HFD for 8 weeks. Total adiponectin, n = 8–17; HMW adiponectin, n = 7–11. One-way ANOVA with Dunnett’s test.

(B) WB analysis of adiponectin in the serum of WT and *Becl1*^{F121A} mice fed with HFD for 8 weeks. n = 6.

(C) ELISA of serum adiponectin in WT littermates (+/+) and *Becn1*^{+/-} KO (+/-) mice fed with HFD for 8 weeks. +/+, n = 12; +/-, n = 10.

(D) Total and HMW adiponectin are increased in *Becn1*^{F121A} mice. WB analysis of HMW and total adiponectin in the serum of WT and *Becn1*^{F121A} mice using a mouse anti-adiponectin antibody (MA1-054; Thermo Fisher Scientific). Total protein loading is shown by Ponceau S staining. n = 7.

(E) *Becn1*^{F121A}-induced adiponectin secretion is cell autonomous. Primary adipocytes (adipose-derived stromal vascular fraction [SVF] cells) isolated from *Becn1*^{F121A} mice secrete more adiponectin into the conditioned medium than those from WT mice, quantified by WB analysis after 24-h culture. Total protein loading is shown by Ponceau S staining. n = 3 mice.

Data represent mean ± SEM, t test. *p < 0.05; **p < 0.01; ***p < 0.001.

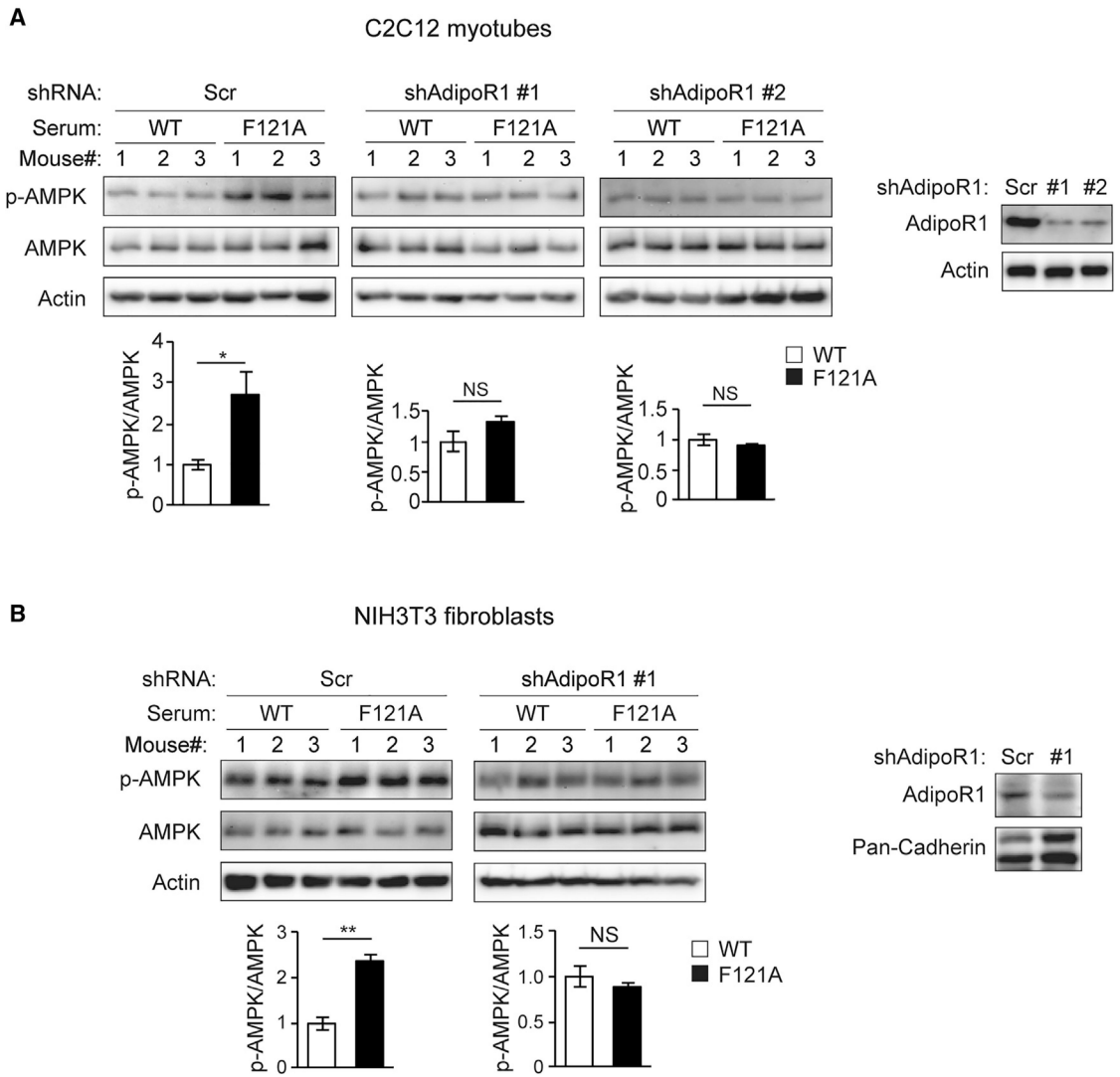


Figure 3. Non-cell-autonomous activation of AMPK by *Becn1*^{F121A} mouse serum is mediated by adiponectin signaling

(A and B) C2C12 myotubes (A) or NIH 3T3 fibroblasts (B) stably expressing scrambled (Scr) or shRNAs against adiponectin receptor 1 (AdipoR1) were cultured for 1 h in medium containing 10% mouse serum from WT or *Becn1*^{F121A} mice, and AMPK phosphorylation was analyzed and quantified by WB studies. AdipoR1 KD efficiency is shown on the right. n = 3 mice.

Data represent mean ± SEM, t test. *p < 0.05; **p < 0.01. NS, not significant.

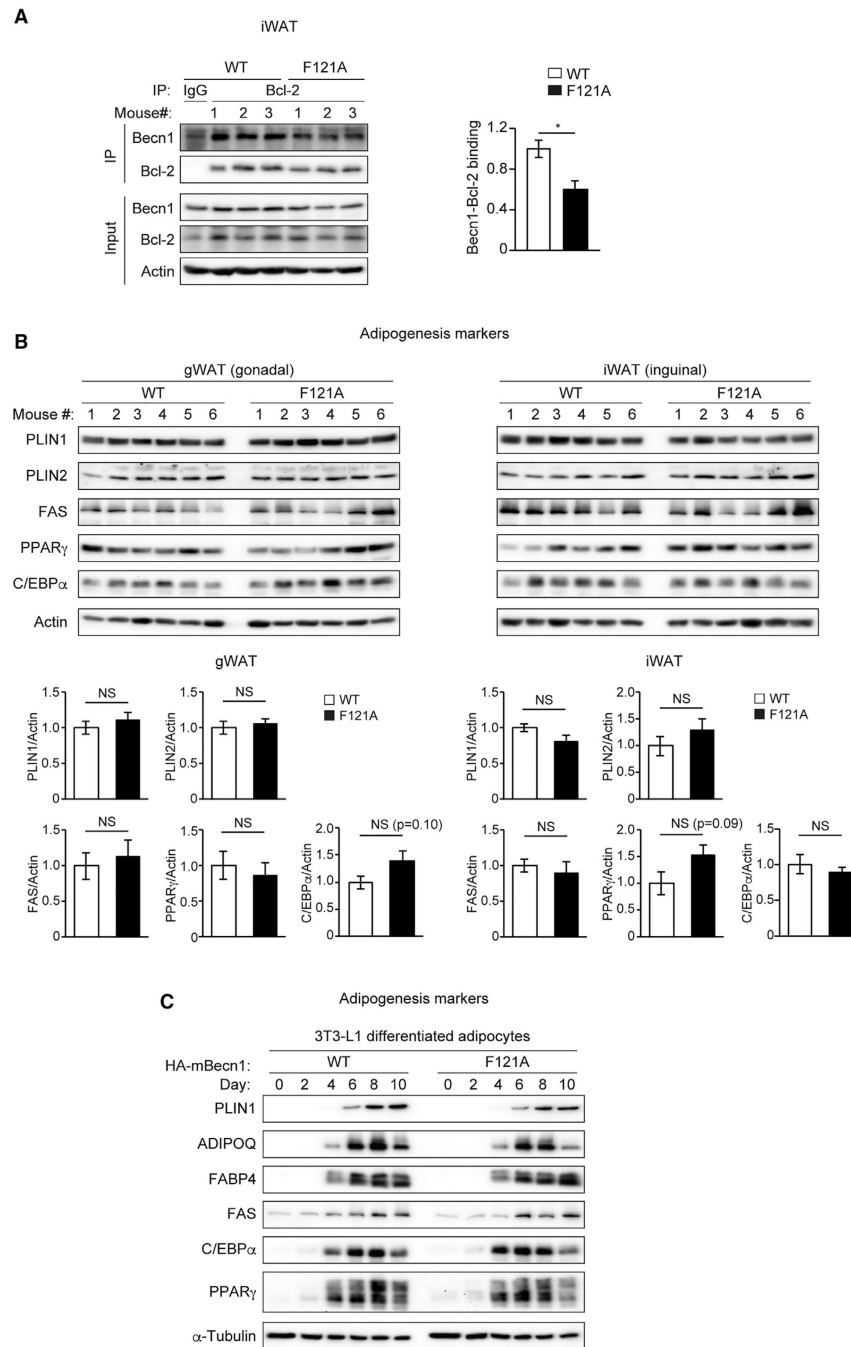


Figure 4. Increasing autophagy by Becn1^{F121A} does not promote adipogenesis *in vivo* or *in vitro* (A) CoIP of endogenous Bcl-2 and Becn1 in the iWAT of WT and Becn1^{F121A} mice. n = 3 mice.

(B) Adipogenesis markers in gWAT and iWAT of RD-fed WT and Becn1^{F121A} mice were analyzed by WB. n = 6 mice. t test. Data represent mean \pm SEM.

(C) 3T3-L1 preadipocytes stably expressing hemagglutinin (HA)-tagged WT Becn1 or Becn1^{F121A} were cultured in the adipocyte-differentiation medium for a 10-day time course, and adipogenesis markers were analyzed every 2 days by WB.

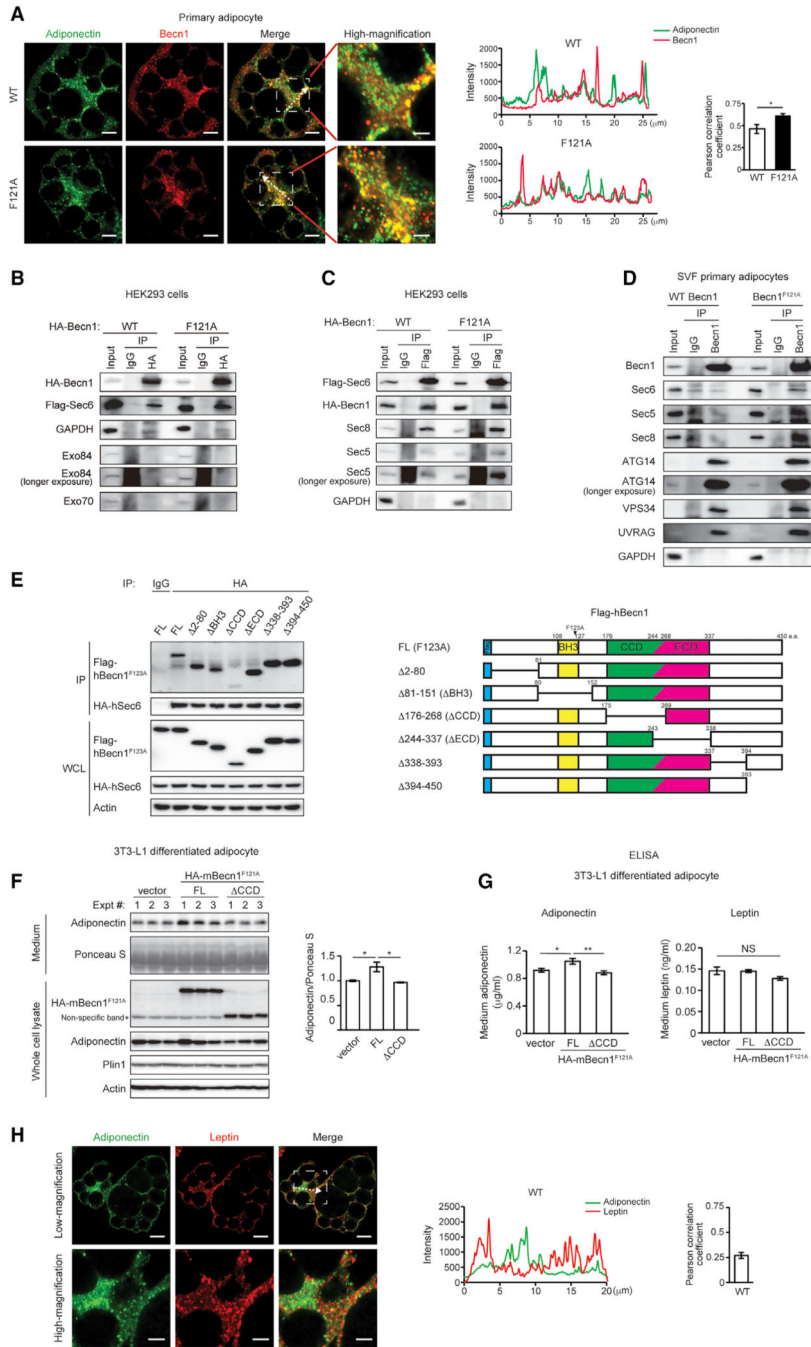


Figure 5. Becn1 forms a complex with the exocyst, and the Becn1-exocyst interaction is essential to increase secretion of adiponectin, but not leptin, in Becn1^{F121A} adipocytes

(A) Immunofluorescence staining of adiponectin (green) and Becn1 (red) in SVF primary adipocytes isolated from WT or Becn1^{F121A} mice. The intensity line profile measurements show intensity distribution on dashed arrows in the images above. Pearson correlation coefficient is used to quantify colocalization between adiponectin and Becn1. Low magnification, scale bars: 10 μm; high magnification, scale bars: 5 μm. n = 7 cells. t test.

(B) The exocyst component Sec6, but not Exo84 or Exo70, is pulled down by Becn1^{F121A} more strongly than WT Becn1. CoIP of FLAG-Sec6 by HA-Becn1 in HEK293 cells transfected with Sec6 and WT Becn1 or Becn1^{F121A}.

(C) Becn1^{F121A} promotes exocyst assembly. CoIP of HA-Becn1, Sec8, and Sec5 by FLAG-Sec6 in HEK293 cells transfected with Sec6 and WT Becn1 or Becn1^{F121A}.

(D) CoIP of endogenous exocyst components (Sec6, Sec5, and Sec8) and autophagy-related PtdIns3K proteins (Atg14, Vps34, and UVRAG) with the endogenous Becn1 protein in primary adipocytes isolated from WT or Becn1^{F121A} mice. One-way ANOVA with Tukey-Kramer test.

(E) CoIP of HA-hSec6 (human Sec6) and indicated full-length (FL) and deletion mutants of FLAG-hBecn1^{F123A} (human Becn1^{F123A}, mouse Becn1^{F121A} equivalent) in HEK293 cells.

(F) WB analysis of adiponectin levels in the conditioned medium secreted from WT 3T3-L1-differentiated adipocytes stably expressing HA-tagged FL Becn1^{F121A} or the Becn1^{F121A}

CCD deletion mutant after 24-h culture. Intracellular adiponectin and total protein loading (Ponceau S staining) are also shown. n = 3.

(G) ELISA of adiponectin and leptin in the conditioned medium of WT 3T3-L1-differentiated adipocytes stably expressing HA-tagged FL Becn1^{F121A} or the Becn1^{F121A}

CCD deletion mutant after 24-h culture. n = 6.

(H) Leptin and adiponectin vesicle pools have limited colocalization in adipocytes.

Immunofluorescence staining of adiponectin and leptin in primary adipocytes of WT mice. Low magnification, scale bars: 10 μ m; high magnification, scale bars: 5 μ m. n = 12 regions. Data represent mean \pm SEM. One-way ANOVA with Tukey-Kramer test. *p < 0.05; **p < 0.01.

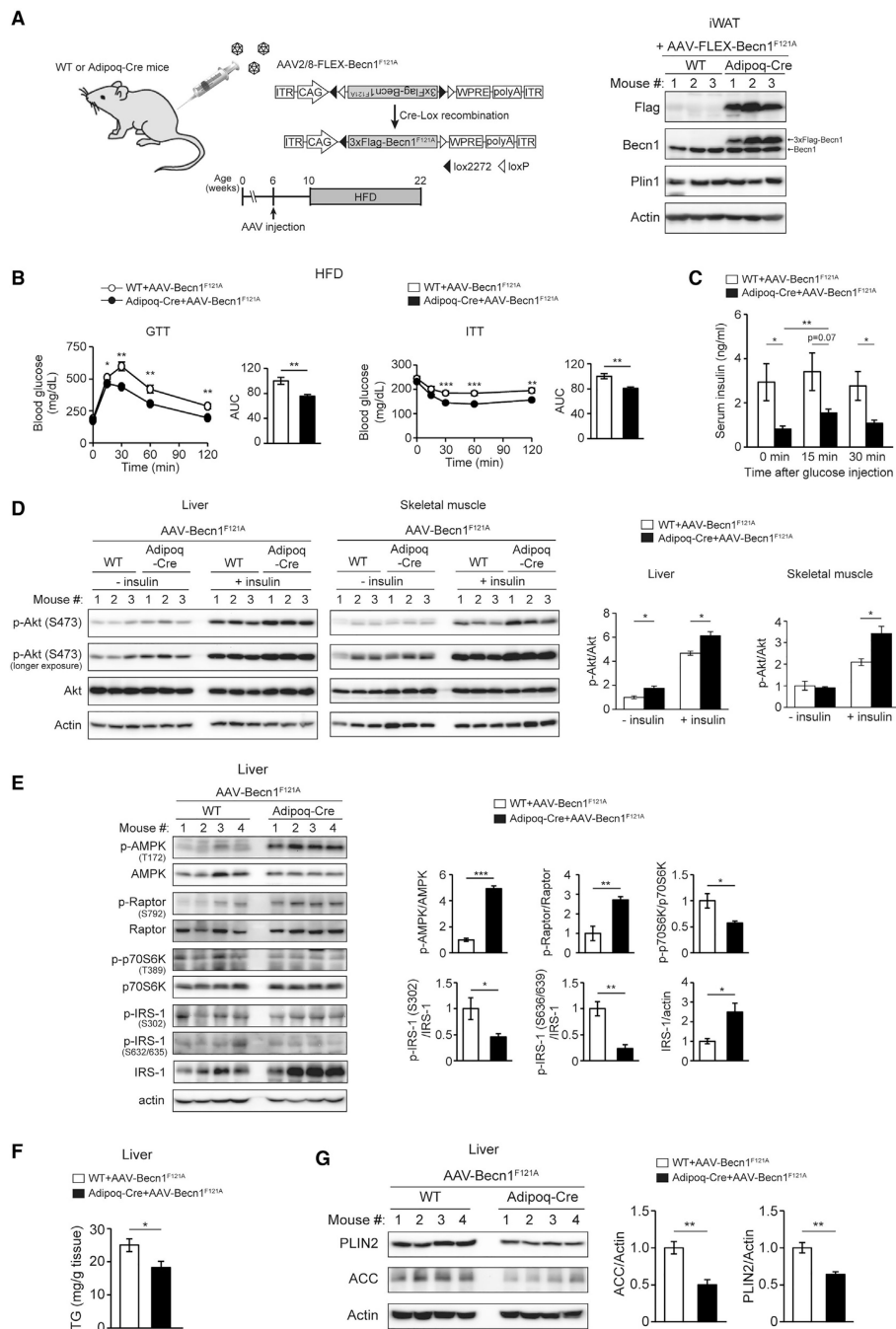


Figure 6. Adipose-specific Beclin^{F121A} improves both insulin sensitivity and glucose tolerance and regulates insulin signaling, AMPK activity, and lipid metabolism in non-adipose tissues

(A) Adipose-specific expression of Beclin^{F121A} via injection of AAV2/8-FLEX-3XFlag-Beclin^{F121A} to Adipoq-Cre mice.

(B) GTT and ITT in Adipoq-Cre or control (WT) mice injected with AAV2/8-FLEX-3XFlag-Beclin^{F121A} and then fed with HFD for 12 weeks. WT+AAV-Becn1^{F121A}, n = 11; Adipoq-Cre+AAV-Becn1^{F121A}, n = 9.

(C) ELISA of serum insulin levels before and after intraperitoneal (i.p.) glucose injection in Adipoq-Cre or control (WT) mice injected with AAV2/8-FLEX-3XFlag-Beclin^{F121A} and fed

with HFD for 12 weeks. WT+AAV-Becn1^{F121A}, n = 11; Adipoq-Cre+AAV-Becn1^{F121A}, n = 9. One-way ANOVA with Tukey-Kramer test.

(D) WB analysis of insulin-induced Akt phosphorylation in the liver and muscle of Adipoq-Cre or control (WT) mice injected with AAV2/8-FLEX-3XFlag-Becn1^{F121A} and fed with HFD for 12 weeks. n = 3. t test.

(E) WB analysis of AMPK activation and signaling pathways downstream of AMPK in the liver of Adipoq-Cre or WT mice injected with AAV2/8-FLEX-Becn1^{F121A} and then fed with HFD for 12 weeks. n = 4. t test.

(F) TG levels in the liver of Adipoq-Cre or WT mice injected with AAV2/8-FLEX-Becn1^{F121A} and then fed with HFD for 12 weeks. WT+AAV-Becn1^{F121A}, n = 12; Adipoq-Cre+AAV-Becn1^{F121A}, n = 9. t test.

(G) WB analysis of PLIN2 and ACC in the liver of Adipoq-Cre or WT mice injected with AAV2/8-FLEX-Becn1^{F121A} and then fed with HFD for 12 weeks. n = 4.

Data represent mean \pm SEM, t test. *p < 0.05; **p < 0.01; ***p < 0.001. AUC, area under the curve.

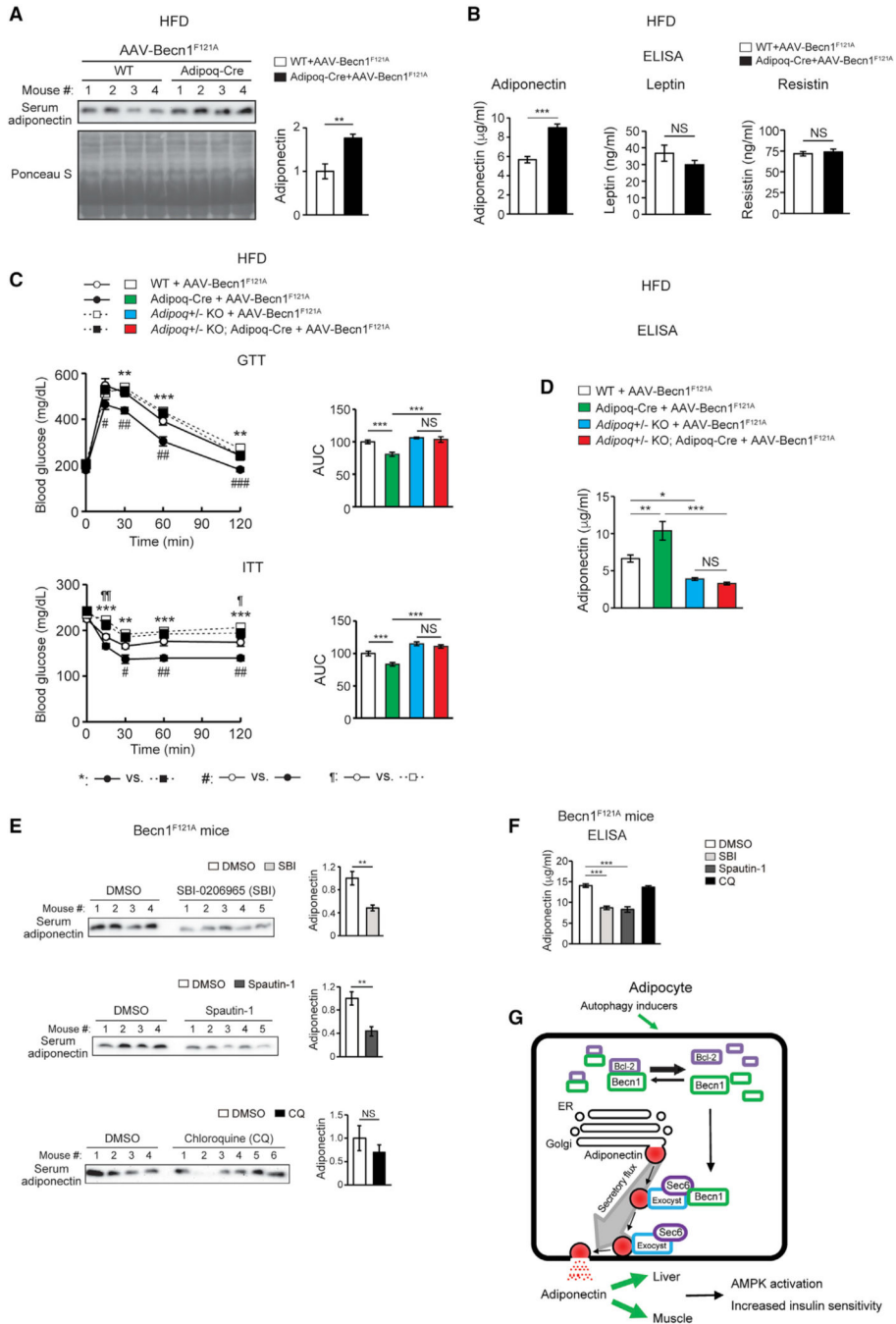


Figure 7. Adipose-specific Becn1^{F121A} non-cell-autonomously improves systemic insulin sensitivity via promoting adiponectin secretion

(A) WB analysis of serum adiponectin levels in Adipoq-Cre or control (WT) mice injected with AAV2/8-FLEX-Becn1^{F121A} and then fed with HFD for 12 weeks. n = 4. t test.

(B) ELISA of serum levels of adiponectin, resistin, and leptin in Adipoq-Cre or WT mice injected with AAV2/8-FLEX-Becn1^{F121A} and then fed with HFD for 12 weeks. WT+AAV-Becn1^{F121A}, n = 11; Adipoq-Cre+AAV-Becn1^{F121A}, n = 9. t test.

(C and D) Reducing adiponectin in adipose-specific Becn1^{F121A} mice abolishes the insulin-sensitizing effects of adipose Becn1^{F121A}. GTT and ITT (C) and ELISA of serum

adiponectin (D) of WT and adipose-specific *Becn1*^{F121A} mice expressing both or one copy of *Adiponectin* after 8 weeks of HFD feeding. For GTT and ITT: WT+AAV-*Becn1*^{F121A}, n = 9; Adipoq-Cre+AAV-*Becn1*^{F121A}, n = 9; *Adipoq*^{+/-} KO+AAV-*Becn1*^{F121A}, n = 6; *Adipoq*^{+/-} KO Adipoq-Cre+AAV-*Becn1*^{F121A}, n = 5. For adiponectin ELISA: n = 5–6. One-way ANOVA with Dunnett's test.

(E) Inhibiting early (upper), but not late (lower), stages of autophagy reduces adiponectin release to circulation in mice. WB analysis of adiponectin in the serum of HFD-fed *Becn1*^{F121A} mice treated with SBI-0206965 (SBI) or Spautin-1 (early-stage inhibitors, inhibiting autophagosome formation) or chloroquine (CQ; late-stage inhibitor, inhibiting lysosomal degradation). n = 4–6. t test.

(F) ELISA of serum adiponectin in HFD-fed *Becn1*^{F121A} mice treated with SBI-0206965, Spautin-1, or CQ. n = 5–8. One-way ANOVA with Dunnett's test. Data represent mean ± SEM. *,#,#,¶p < 0.05; **,##,¶¶p < 0.01; ***,###,¶¶¶p < 0.001.

(G) Model of *Becn1*-regulated adiponectin secretion. When the essential autophagy protein *Becn1* is released from its inhibitor Bcl-2 in adipose tissue, triggered by exercise or the active *Becn1*^{F121A} mutation, it interacts with Sec6 and other exocyst components to increase adiponectin secretion, systemic AMPK activation, and insulin sensitivity.

KEY RESOURCES TABLE

REAGENT or RESOURCE	SOURCE	IDENTIFIER
Antibodies		
anti-LC3B	Novus Biologicals	Cat#NB100-2220; RRID:AB_10003146
anti-Leptin	Novus Biologicals	Cat#NB300-611; RRID:AB_2136214
anti-TLR9	Novus Biologicals	Cat#NBP2-24729
anti-p62	BD Biosciences	Cat#610833; RRID:AB_398152
anti-PLIN2	Progen	Cat#GP40
anti-acetyl-CoA carboxylase	Cell Signaling Technology	Cat#3676; RRID:AB_2219397
anti-fatty acid synthase	Cell Signaling Technology	Cat#3180; RRID:AB_2100796
anti-PPAR γ	Cell Signaling Technology	Cat#2435; RRID:AB_2166051
anti-C/EBP α	Cell Signaling Technology	Cat#8178; RRID:AB_11178517
anti-PLIN1	Cell Signaling Technology	Cat#9349; RRID:AB_10829911
anti-AMPK	Cell Signaling Technology	Cat#2532; RRID:AB_330331
anti-phospho-AMPK (Thr172)	Cell Signaling Technology	Cat#2535; RRID:AB_331250
anti-phospho-AMPK (Thr172)	Cell Signaling Technology	Cat#2531; RRID:AB_330330
anti-Raptor	Cell Signaling Technology	Cat#2280; RRID:AB_561245
anti-phospho-Raptor (Ser792)	Cell Signaling Technology	Cat#2083; RRID:AB_2249475
anti-p70S6K	Cell Signaling Technology	Cat#2708; RRID:AB_390722
anti-phospho-p70S6K (Thr389)	Cell Signaling Technology	Cat#9234; RRID:AB_2269803
anti-IRS-1	Cell Signaling Technology	Cat#3407; RRID:AB_2127860
anti-phospho-IRS-1 (Ser302)	Cell Signaling Technology	Cat#2491; RRID:AB_823551
anti-phospho-IRS-1 (Ser636/639)	Cell Signaling Technology	Cat#2388; RRID:AB_330339
anti-Akt	Cell Signaling Technology	Cat#4691; RRID:AB_915783
anti-phospho-Akt (Ser473)	Cell Signaling Technology	Cat#4060; RRID:AB_2315049
anti-ATG14	MBL International	Cat#PD026; RRID:AB_1953054
anti-UVRAG	Millipore Sigma	Cat#SAB4200005; RRID:AB_10603351
anti-GFP	Millipore Sigma	Cat#G1544; RRID:AB_439690
horseradish peroxidase (HRP)-conjugated anti-Flag M2	Millipore Sigma	Cat#A8592; RRID:AB_439702
anti-VPS34 antibody	Echelon Biosciences	Cat#Z-R016; RRID:AB_11128208
anti-GAPDH	Thermo Fisher Scientific	Cat#MA5-15738; RRID:AB_10977387
anti-Phospho-IRS1 (Tyr612)	Thermo Fisher Scientific	Cat#44-816G; RRID:AB_2533768
anti-BECN1	Santa Cruz Biotechnology	Cat#sc-11427; RRID:AB_2064465
anti-BECN1	Santa Cruz Biotechnology	Cat#sc-48341; RRID:AB_626745
anti- α -Tubulin	Santa Cruz Biotechnology	Cat#sc-53029; RRID:AB_793541
anti-Bcl-2	Santa Cruz Biotechnology	Cat#sc-7382; RRID:AB_626736
HRP-conjugated anti- β -Actin	Santa Cruz Biotechnology	Cat#sc-47778 HRP; RRID:AB_2714189
anti-SEC6	Santa Cruz Biotechnology	Cat#sc-374054; RRID:AB_10916711
anti-SEC5	Santa Cruz Biotechnology	Cat#sc-393230
anti-SEC8	Santa Cruz Biotechnology	Cat#sc-514215
anti-EXO84	Santa Cruz Biotechnology	Cat#sc-515532

REAGENT or RESOURCE	SOURCE	IDENTIFIER
anti-EXO70	Santa Cruz Biotechnology	Cat#sc-365825; RRID:AB_10843358
anti-AdipoR1	Santa Cruz Biotechnology	Cat#sc-518030
anti-HA	Cell Signaling Technology	Cat#3724; RRID:AB_1549585
anti-HA	Santa Cruz Biotechnology	Cat#sc-7392; RRID:AB_627809
anti-adiponectin	Cell Signaling Technology	Cat#2789; RRID:AB_2221630
anti-adiponectin	Thermo Fisher Scientific	Cat#MA1-054; RRID:AB_557516
HRP-conjugated anti-rabbit IgG	Jackson ImmunoResearch Labs	Cat#111-035-003; RRID:AB_2313567
HRP-conjugated anti-mouse IgG	Jackson ImmunoResearch Labs	Cat#115-035-003; RRID:AB_10015289
HRP-conjugated anti-guinea pig IgG	Thermo Fisher Scientific	Cat#A18769; RRID:AB_2535546
Alexa Fluor 594-conjugated anti-mouse IgG	Thermo Fisher Scientific	Cat#A-11005 RRID:AB_2534073
Alexa Fluor Plus 488-conjugated anti-mouse IgG	Thermo Fisher Scientific	Cat#A32723; RRID:AB_2633275
Alexa Fluor Plus 594-conjugated anti-rabbit IgG	Thermo Fisher Scientific	Cat#A32740; RRID:AB_2762824
Mouse IgG Isotype Control	Thermo Fisher Scientific	Cat#02-6502; RRID:AB_2532951
Bacterial and virus strains		
Lentivirus: shRNA (pLKO.1)	This paper	N/A
Retrovirus: GFP-LC3	This paper	N/A
Adeno-associated virus (AAV): CAG-FLEX-3xFlag-mBECN1 ^{F121A}	This paper	N/A
Lentivirus: HA-tagged mouse BECN1 (HA-mBECN1)	This paper	N/A
Chemicals, peptides, and recombinant proteins		
Dexamethasone	Millipore Sigma	Cat#D4902; CAS: 50-02-2
Polybrene	Millipore Sigma	Cat#TR-1003-G
anti-Flag M2 affinity gel	Millipore Sigma	Cat#A2220
Type I collagenase	Worthington Biomedical Corp.	Cat#LS004196
Type II collagenase	Worthington Biomedical Corp.	Cat#LS004176
3-isobutyl-1-methylxanthine (IBMX)	MP biomedical	Cat#195262; CAS: 28822-58-4
Rosiglitazone	Tokyo Chemical Industry Co.	Cat#R0106; CAS: 122320-73-4
Halt Protease and Phosphatase inhibitor cocktail	Thermo Fisher Scientific	Cat#78446
ProLong Diamond Antifade Mountant	Thermo Fisher Scientific	Cat#P36961
Lipofectamine 3000 transfection reagent	Thermo Fisher Scientific	Cat#L3000150
PowerUP SYBR Green Master Mix	Thermo Fisher Scientific	Cat#A25742
Protein A/G Plus-Agarose	Santa Cruz Biotechnology	Cat#sc-2003
IgG Sepharose 6 Fast Flow	Cytiva	Cat#17-0969-01
ProTEV Plus	Promega	Cat#V6101
SBI-0206965	ApexBio	Cat#A8715; CAS: 1884220-36-3
DNase I	Millipore Sigma	Cat#D5025; CAS: 9003-98-9
AICAR	Cayman Chemical	Cat#10010241; CAS: 2627-69-2
Infinity Triglycerides Liquid Stable Reagent	Thermo Fisher Scientific	Cat#TR22421
SapphireAmp Fast PCR Master Mix	Takara Bio Inc.	Cat#RR350B
Spautin-1	AdooQ Bioscience	Cat#A12942; CAS: 1262888-28-7

REAGENT or RESOURCE	SOURCE	IDENTIFIER
Chloroquine (phosphate)	Cayman Chemical	Cat#14194; CAS: 50-63-5
Insulin	Millipore Sigma	Cat#I0516-5ML; CAS: 11070-73-8
Histopaque-1077	Millipore Sigma	Cat#10771
Critical commercial assays		
Mouse HMW & Total Adiponectin ELISA	ALPCO	Cat#47-ADPMS-E01
Mouse Adiponectin/Acrp30 DuoSet ELISA	R&D Systems	Cat#DY1119
Ultra Sensitive Mouse Insulin ELISA Kit	Crystal Chem	Cat#90080
Mouse Leptin DuoSet ELISA	R&D Systems	Cat#DY498-05
Mouse Resistin ELISA Kit	RayBiotech, Inc.	Cat#ELM-Resistin-1
Mouse/Rat FGF-21 ELISA Kit	Proteintech	Cat#KE10042
In-Fusion HD cloning Plus kit	Takara Bio Inc.	Cat#638910
BCA protein assay kit	Thermo Fisher Scientific	Cat#23225
High-Capacity cDNA Reverse Transcription kit	Thermo Fisher Scientific	Cat#4368814
Experimental models: Cell lines		
Human: HEK293 cells	ATCC	Cat#CRL-1573
Human: HEK293FT cells	Thermo Fisher Scientific	Cat#R70007
Human: T-Rex 293 cells	Thermo Fisher Scientific	Cat#R71007
Human: GP2-293 cells	Takara Bio Inc.	Cat#631458
Human: WI-38 cells	ATCC	Cat#CCL-75
Human: Huh7 cells	JCRB Cell Bank	Cat#JCRB0403
Mouse: 3T3-L1 cells	ATCC	Cat#CL-173
Human: HepG2 cells	ATCC	Cat#HB-8065
Mouse: NIH 3T3 cells	ATCC	Cat#CRL-1658
Mouse: C2C12 cells	ATCC	Cat#CRL-1772
Experimental models: Organisms/Strains		
Mouse: <i>Becn1</i> ^{F121A} knockin mice: B6.129(Cg)- <i>Becn1</i> ^{tm1.1Hec/J}	The Jackson Laboratory	Cat#033360
Mouse: Adipoq-Cre: B6.FVB-Tg(Adipoq-cre)1Evdrl/J	The Jackson Laboratory	Cat#028020
Mouse: Adipoq KO: B6;129- <i>Adipoq</i> ^{tm1Chan/J}	The Jackson Laboratory	Cat#008195
Mouse: <i>Becn1</i> heterozygous KO mice: B6.129X1- <i>Becn1</i> ^{tm1Blev/J}	The Jackson Laboratory	Cat#018429
Mouse: GFP-LC3 mice: Tg(CAG-EGFP/Map1lc3b)53Nmz	RIKEN BioResource Research Center	Cat#RBRC00806
Mouse: C57BL/6J mice	The Jackson Laboratory	Cat#000664
Oligonucleotides		
Primers for shRNA, see Table S1	This paper	N/A
Primers for PCR, see Table S2	This paper	N/A
Recombinant DNA		
pcDNA3.1(-)	Thermo Fisher Scientific	Cat#V79520

REAGENT or RESOURCE	SOURCE	IDENTIFIER
pCDH-CMV-MCS-EF1-Puro	System Biosciences	Cat#CD510B-1
BECLIN-HA WT	Russell et al., 2013	Addgene plasmid Cat#46993; RRID:Addgene_46993
pLKO.1 - TRC cloning vector	Moffat et al., 2006	Addgene plasmid Cat #10878; RRID:Addgene_10878
pLKO.1 scramble shRNA	Sarbassov et al., 2005	Addgene plasmid Cat #1864; RRID:Addgene_1864
pCMV-VSV-G	Stewart et al., 2003	Addgene plasmid Cat #8454; RRID:Addgene_8454
psPAX2	Gift of Didier Trono lab	Addgene plasmid Cat #12260; RRID:Addgene_12260
pBABEpuro GFP-LC3	Fung et al., 2008	Addgene plasmid Cat #22405; RRID:Addgene_22405
pAAV-FLEX-GFP	Gift of Edward Boyden lab	Addgene plasmid Cat #28304; RRID:Addgene_28304
pZZ-Flag	Sun et al., 2008	N/A
pAAV-FLEX-3xFlag-mBecn1 ^{F121A}	This Paper	N/A
pcDNA3.1 (-) HA-hSec6	This Paper	N/A
pcDNA3.1 (-) Flag-hBECN1	This Paper	N/A
pCDH-Flag-hSec6	This Paper	N/A
pCDH-HA-hBECN1	This Paper	N/A
pCDH-HA-mBECN1	This Paper	N/A
Software and algorithms		
ImageJ	National Institutes of Health	https://imagej.nih.gov/ij/
NIS-Elements	Nikon	https://www.microscope.healthcare.nikon.com/products/software/nis-elements